Applied Surface Science Advances 5 (2021) 100097

Contents lists available at ScienceDirect

Applied Surface Science Advances

journal homepage: www.elsevier.com/locate/apsadv

Monolayer colloidal lithography protocol: theoretical assessment and applicative potentialities for metal nanohole fabrication

Maura Cesaria[a,b,†], Antonietta Taurino[a,*], Maria Grazia Manera[a], Simona Scarano[b], Maria Minunni[b], Roberto Rella[a]

[a] Institute for Microelectronics and Microsystems, IMM-CNR, Via Monteroni, Lecce I-73100, Italy
[b] Università degli Studi di Firenze, Department of Chemistry "Ugo Schiff", Via della Lastruccia 3-13, Sesto Fiorentino 50019, Italy

ARTICLE INFO

Keywords:
Monolayer colloidal lithography protocol
Threshold interparticle-spacing model
Autocorrelation analysis
Salt-related degraded ordering
Refractive index sensing

ABSTRACT

Polystyrene colloids adsorbed onto a poly(diallyldimethylammonium chloride) (PDDA) monolayer is the model-system exploited to present and discuss both theoretical assessment and extended practical roadmap of the monolayer colloidal lithography (MNL-CL) protocol, recently developed by the authors to efficiently simplify and speed-up the deposition of template colloidal masks. Advantages of the MNL-CL protocol are demonstrated, in terms of ordering and coverage optimization of colloid arrangements, over the entire coverage range of its application, that is even under the commonly disregarded unsaturated adsorption conditions.

A conceptual model is presented predicting an interparticle threshold spacing below which the impact of the polyelectrolyte binding surface on colloidal arrangement, degree of ordering and coverage may be observed. This discussion discloses the key interplay between the critical working parameters (mainly deposition times of PDDA and colloids as well as salt-induced screening of the intercolloid repulsion) allowing optimal design of colloidal arrangements in terms of order, homogeneity and coverage. In this respect, the occurrence of correlated disorder with respect to disordered arrangements is rigorously characterized by quoting a periodicity-like length associated to the real colloidal distributions.

Finally, we perform optical and sensing characterization of metal nanohole distributions with tailored short-range ordering fabricated by the MNL-CL protocol.

1. Introduction

Nanoplasmonics is a field of active applicative interest and fundamental research that exploits the ability of metallic nanostructures (nanoparticles and nanoholes) to confine light at the nanoscale and probe small changes in the dielectric and biologic environment close to a noble metal surface [1-4]. Unique physical and optical properties of noble metals are associated with surface plasmon resonance (SPR) phenomena, arising from resonant (at the plasma frequency) interaction between electromagnetic external fields and conduction electrons on the metal surface [5]. In general, the enhancement of the SPR evanescent field is exploited in numerous applications, like surface enhanced spectroscopies [6-8], biosensors [9-11], chemical sensors [2], and optical devices [12-14]. Depending on geometry (i.e., film- or nanoparticle-like) and nanostructuring (i.e., nanoparticle or nanohole distributions) of the metal-dielectric interface, plasmonic waves with propagating nature (surface plasmon polaritons (SPP)) and/or localized nature (localized SPR (LSPR)) can be excited [15-18]. From the sensing standpoint, sensitivity to molecular adsorption events is the main difference between localized and propagating modes, stemming from the different confinement scale and intensity enhancement of the plasmonic fields [19].

Recently, the simultaneous excitation of propagating and localized plasmon modes supported by nanohole arrays has demonstrated to combine the advantages of SPPs and LSPRs, leading to superior bulk sensitivity and detection limits of molecular events [20,21].

In this appealing applicative scenario, fabrication techniques of plasmonic systems providing repeatable and nearly defect-free nanostructuring with controllable features (size, shape, inter-particle spacing, composition, surrounding dielectric) are demanding. In this respect, top-down nanofabrication techniques able to achieve high reproducibility, fine nano-processing performances and ultimate resolution of a few nanometers are scanning beam lithographic methods [22], namely electron beam lithography [23,24] and focused ion beam lithography [25].

* Corresponding author.
E-mail address: antonietta.taurino@cnr.it (A. Taurino).
† Present Address: Department of Mathematics and Physics "Ennio De Giorgi", University of Salento, prov. le Arnesano, 73100, Lecce, Italy.

https://doi.org/10.1016/j.apsadv.2021.100097
Received 26 November 2020; Received in revised form 19 March 2021; Accepted 4 April 2021

However, they are expensive time-consuming techniques using specialized equipment and more suitable for controlled fabrication over small areas (~100 × 100 μm^2). These limitations have prompted the development of "natural lithography" (nanosphere lithography and colloidal lithography) as alternative, inexpensive, inherently parallel, high-throughput, mask-assisted approaches for manufacturing either highly ordered or short-range ordered arrays of nanoparticles and nanoholes over large areas (~cm^2) [26-29].

Colloidal lithography relies on electrostatically-[30-33] or capillary-driven [28,34-36] self-assembling onto an interface (liquid-solid or liquid-liquid) of colloids with diameter in the micrometer to nanometer range. Operative advantages are: i) monodisperse colloids with desired composition, surface charge and size can be routinely synthesized via wet chemistry at low cost, ii) a broad choice of colloids is available commercially, iii) mask preparation is a very rapid and cost-effective step, iv) colloidal masks can be easily lifted-off by tape stripping without wet etching processes and v) masks can be post-processed without affecting their arrangement [36-40].

The collector surface used for electrostatic anchoring of the colloids is usually a polyelectrolyte multilayer, preliminary deposited by the so-called layer-by-layer method [41-44] that consists of solution-based deposition of alternating positively and negatively charged polyelectrolytes leading to an uppermost surface charge opposite to the one of the mutually repelling likely-charged colloids [31,45,46].

Chain conformation and chain interpenetration of the counter-charged polyelectrolytes, resulting from polyelectrolytes type and experimental conditions (salt type and content, polyelectrolyte concentration, pH and solvent of the solution, deposition time), play a significant role [41,45,47,48]. Layer-by-layer method is quite time-consuming because deposition lasting from a few minutes to tens of minutes is applied for each layer to achieve saturated thickness and stable reconfiguration of the polymer chains as well as charge overcompensation [41,47,49,50]. In addition, as saturated coverage and uniformity of colloidal arrangements is favoured by increasing number (at least seven layers) of the polyelectrolyte layers [46], colloidal lithography using the layer-by-layer method is more and more time- and material-consuming.

Modeling of colloidal adsorption demonstrated that the range of inter-particle electrostatic interactions and the zeta potential of the collector surface effectively control final fractional coverage and ordering, respectively [51]. Therefore, in principle, an adsorptive surface able to effectively bind the colloids is required, which could not be a polyelectrolyte multilayer. Then, using a polyelectrolyte monolayer would undoubtedly simplify the lithography protocol. To the best of our knowledge, this possibility was not investigated properly in the literature [31,52-55].

Recently, the authors demonstrated the effectiveness of using a smooth polydiallyldimethylammonium (PDDA) monolayer for the fabrication of gold short-range ordered nanoholes as large-area optical transducers in sensing applications [56,57]. Such modified colloidal lithography protocol (briefly termed monolayer colloidal lithography (MNL-CL) protocol hereafter, where MNL and CL stands for "monolayer" and "colloidal lithography", respectively) was demonstrated to efficiently simplify and speed-up the conventional colloidal lithography procedure exploiting polyelectrolyte multilayers.

Going deep insight the presentation of the MNL-CL protocol and the associated conceptual and practical raised questions, two main issues were worth further investigation. The first one was the assessment of a lattice-like model for a correct interpretation of the transmission resonances of short-range ordered nanoholes [58]. The second issue was the theoretical assessment and general applicability of the MNL-CL protocol that was demonstrated for designing gold nanohole arrangements with specific variation of the nanohole-to-nanohole distance [56,57].

In this paper, on the basis of the missing information in our recent publications, we present extended investigation and unprecedented discussion, focusing on the following main aspects:

i) the theoretical assessment of the MNL-CL protocol through physical insight in the underlying physical processes by developing a simple conceptual model predicting a threshold interparticle spacing below which the impact of the polyelectrolyte layer on the colloid distribution may be probed and, consequently, exploited in fabricating colloidal masks,
ii) potentialities of the MNL-CL protocol in terms of ordering optimization of the colloidal arrangement over the entire coverage range of its application, and
iii) comprehensive demonstration of its ability to describe the applicative limits of salt-screening, commonly used to increase coverage, and the degree of correlated disorder, below a threshold interparticle distance.

Points i) to iii) are key in the optimization of colloidal lithography masks to be used as templates for the fabrication of short-range ordered nanohole distribution with controlled degree of ordering [56-58]. Occurrence of correlated disorder being critical, a rigorous analysis is carried out, by autocorrelation and Fast Fourier processing of SEM images, of the colloidal distributions manufactured by the MNL-CL protocol. On this basis it is demonstrated that, in practice, using salt-free colloidal suspensions is a simple and effective strategy to exploit the interplay between adsorption/deposition times to tune coverage over a wide range of values, while retaining short-range ordering properties.

Finally, practical implications and potentialities of our optimization protocol are demonstrated by spectral characterization and sensing performances of gold nanohole distributions.

2. Experimental

2.1. Materials and methods

Carefully cleaned (by successive ultra-sonication in acetone and isopropanol at 60 °C for 15 min) 1.5 × 1.5 cm^2 glass substrates were subjected to an oxygen plasma treatment (100 sccm, 100 Watt, 250 mTorr for 60 s) to induce a negatively charged surface for subsequent electrostatic binding of a positively charged polydiallyldimethylammonium (PDDA) (MW 200,000–350,000, Sigma Aldrich) layer (Fig. 1(a)) through immersion in a salt-free aqueous solution (0.2% in Milli-Q water) for an incubation time Δt_{PDDA}=40 s, 50 s, 1 min, 2 min, 5 min. PDDA covered substrates were rinsed by Milli-Q water, to remove any excess of PDDA, and blow-dryed by N_2 stream. The starting test value Δt_{PDDA}=40 s was set according to other reports in the literature [53,55].

Moreover, in our experiments the absence of salt assures extended chains and the low concentration of the PDDA solution (0.2% wt in Milli-Q water) rules out both formation of globule-like chains and chain conformational changes [59]. In fact, a smooth polyelectrolyte layer is favoured by chains adsorbing in a flat configuration at a liquid-solid interface and a PDDA monolayer deposited from a salt-free polyelectrolyte solution does not change its surface structure under aging [45].

In an aqueous solution, the cationic strong polyelectrolyte PDDA dissociates into negatively charged Cl^- ions and positively charged polymer chains (consisting of hydrophilic amino groups and hydrophobic hydrocarbyl groups) that will act as anchoring points for the negatively charged colloids. Hence, for depositing the colloidal mask (Fig. 1(c)), the PDDA-coated glass substrates (Fig. 1(b)) were immersed in a previously ultra-sonicated suspension of negatively charged polystyrene (PS) beads (Thermo Fisher, concentration C_{PS}= 0.1, 0.2% in Mili-Q water) for an adsorption time Δt_{PS} varying from 25 s to 10 min (Δt_{PS}= 40 s, 50 s, 1 min, 2 min, 5 min, 10 min). The MNL-CL protocol was implemented for colloidal diameter D_{PS}=80 nm, 100 nm accounting for the capillary-induced detrimental agglomeration effects acting for larger diameters, despite of the stronger Coulomb repulsion. Subsequently, all samples were carefully rinsed with Milli-Q water, placed for 1 min in a water bath heated at 100 °C [31] and blow-dried under N_2 stream. The distributions were found to be reproducible.

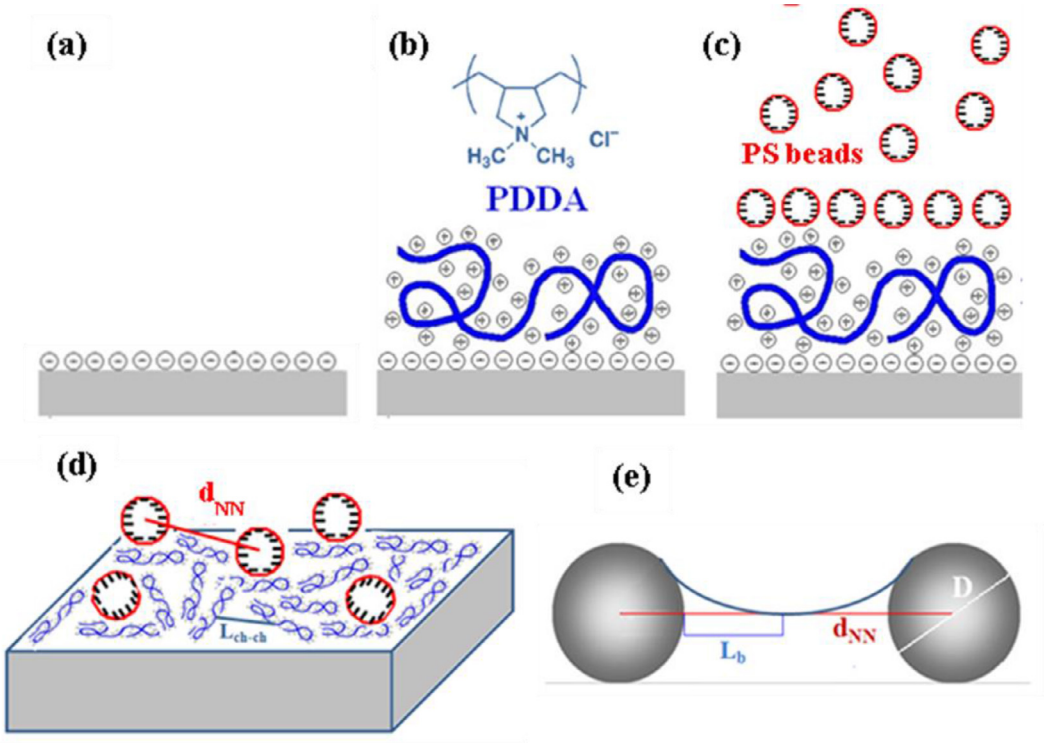

Fig. 1. (Color online) Deposition of a colloidal mask by the MNL-CL protocol. (a) Oxygen-plasma treated glass substrate with negatively induced surface charge. (b) PDDA (with structural formula of a monomer as inset) positively charged monolayer adsorbed onto the functionalized glass substrate. (c) Positively charged PS beads electrostatically adsorbing from an aqueous suspension onto the PDDA monolayer. (d) Sketch of the system (adsorbed polyelectrolyte chains and colloids) with interparticle and interchain spacing d_{NN} and $L_{ch-ch.}$, respectively, in the case $d_{NN} > L_{ch-ch.}$. (e) Definition of the decay length of the electrostatic potential (L_b) associated to a system of two identical repelling spheres with diameter D and charged surface.

Nanohole distributions were fabricated in an optically thin (~20 nm thick) gold film supported onto a glass substrate according to the procedure described elsewhere [56].

Notably, we tested two values of the concentration of the colloidal solution, namely C_{PS}= 0.1, 0.2% wt. Control experiments demonstrated that, under decreasing colloidal size, C_{PS}= 0.1% wt better controls ordering and aggregation up to the saturated adsorption. For instance, turning from 0.1 wt% to 0.2 wt% was found to cause increased tendency to form aggregates even for Δt_{PS} as short as 1 min. Instead, C_{PS}= 0.1% wt was effective in controlling ordering, avoiding aggregation up to the saturated adsorption and thus allowing a finer control of the coverage range versus the adsorption time Δt_{PS}(as it will be discussed). Therefore, in order to fully exploit the potentialities of the MNL-CL protocol, a low enough concentration of the colloidal suspension (i.e., C_{PS}= 0.1% wt) was found to be a proper condition.

The electrostatic repulsion of the colloids was switched from unscreened to screened by sodium chloride (NaCl) salt addition (99.5%, Sigma Aldrich, C_{NaCl} = 2 mM) according to the detailed discussion reported elsewhere [56].

The distributions of Au-capped PS nanospheres and nanoholes deposited from salt-free colloidal suspensions will be referred to as PS(Δt_{PDDA}-Δt_{PS},C_{PS},D_{PS}) and NH(Δt_{PDDA}-Δt_{PS}) respectively, whereas, in presence of salt, the arrangements will be termed PS_{NaCl}(Δt_{PDDA}-Δt_{PS}, C_{PS}, D_{PS}) and NH_{NaCl}(Δt_{PDDA}-Δt_{PS}). All colloidal masks under discussion hereafter are listed in Table 1, where the corresponding experimental conditions are reported according to the adopted nomenclature.

2.2. Characterizations

A Zeiss NVISION 40 dual beam Focused Ion Beam (FIB) system, equipped with a high resolution Gemini electron column, was used for Scanning Electron Microscopy (SEM) imaging. In order to avoid charging effects due to the insulating substrate, the colloidal masks were covered by a thermally evaporated (20±2) nm thick gold (Au) film. Hence, SEM results presented in this study refer to distributions of Au-capped PS colloids mainly. The average inter-particle (center to center) distance between neighboring PS nanospheres (referred to as d_{NN}) was estimated by statistical analysis of the SEM images. The corresponding fractional coverage, hereafter termed cvg, was also estimated and quoted with an uncertainty amounting to nearly 6%.

SEM images were processed by image autocorrelation and Fast Fourier Transform (FFT), according to the method detailed elsewhere [56].

Optically thin perforated gold films obtained by lift-off of the colloidal masks were spectrally investigated by the zero- order transmission curves recorded in air by means of a Cary 500 UV–VIS-NIR spectrometer (Varian, USA). All curves were acquired in the spectral range from 400 to 1000 nm and normalized to a bare cleaned glass substrate.

Sensing performances were measured by tracking the spectral shift $\Delta\lambda$ of the transmission minimum, associated with a propagating plasmon mode, under refractive index (RI) changes upon immersion of the sample in liquid environments with RI increasing from 1.33 (water) to 1.40 (mixtures of glycerol and water). The experimental set-up is detailed elsewhere [56]. Bulk sensitivity was estimated according to the formula $S_b = \Delta\lambda/\Delta RI$.

3. Theoretical assessment of the MNL-CL protocol

Before presenting and discussing our experimental findings, it is appropriate to rationalize the conceptual choice of the experimental conditions selected for the assessment of the MNL-CL protocol. In general, interplay between repulsive inter-particle interactions and attractive particle-adsorptive substrate interactions (depending on the deposition conditions of the polyelectrolyte collector surface, its adsorption

Table 1
Colloidal mask investigated and detail of the experimental conditions corresponding to the adopted nomenclature. The physical meaning of the reported experimental parameters is as follws: Δt_{PDDA} is the adsorption time of the PDDA monolayer, Δt_{PS} is the adsorption time of the colloids, C_{PS} is the concentration of the colloidal suspension, C_{NaCl} is the concentration of NaCl salt and D_{PS} is the colloidal diameter.

Sample	Δt_{PDDA}	Δt_{PS}	C_{PS}	C_{NaCl}	D_{PS}
PS(40s-1 min,0.1%,80 nm)	40 s	1 min	0.1%wt	0 mM	80 nm
PS(1min-1 min,0.1%,80 nm)	1 min	1 min	0.1%wt	0 mM	80 nm
PS(40s-5 min,0.1%,80 nm)	40 s	5 min	0.1%wt	0 mM	80 nm
PS(1min-3 min,0.1%,80 nm)	1 min	3 min	0.1%wt	0 mM	80 nm
PS(2min-1 min,0.1%,80 nm)	2 min	1 min	0.1%wt	0 mM	80 nm
PS_{NaCl}(40s-1 min,0.1%,80 nm)	40 s	1 min	0.1%wt	2 mM	80 nm
PS_{NaCl}(50s-1 min,0.1%,80 nm)	50 s	1 min	0.1%wt	2 mM	80 nm
PS_{NaCl}(1min-25 s,0.1%,80 nm)	1 min	25 s	0.1%wt	2 mM	80 nm
PS_{NaCl}(1min-1 min,0.1%,80 nm)	1 min	1 min	0.1%wt	2 mM	80 nm
PS_{NaCl}(1min-3 min,0.1%,80 nm)	1 min	3 min	0.1%wt	2 mM	80 nm
PS_{NaCl}(1min-5 min,0.1%,80 nm)	1 min	5 min	0.1%wt	2 mM	80 nm
PS_{NaCl}(2min-1 min,0.1%,80 nm)	2 min	1 min	0.1%wt	2 mM	80 nm
PS(40s-1 min,0.1%,100 nm)	40 s	1 min	0.1%wt	0 mM	100 nm
PS(40s-1 min,0.2%,100 nm)	40 s	1 min	0.2%wt	0 mM	100 nm
PS(1min-1 min,0.2%,100 nm)	1 min	1 min	0.2%wt	0 mM	100 nm

efficiency and morphology) drives self-assembling of likely-charged colloids onto an oppositely charged surface (polyelectrolyte collector surface) and may impact on the final distribution of the mask.

Lateral-capillary interaction also plays a role under high-coverage conditions and needs proper strategies to be controlled. For instance, immersion of the just adsorbed colloidal mask in heated water at 100 °C for 1 min (as detailed in the experimental) increases the contact area between the colloids and the collector surface [31]. Such improved colloid-polyelectrolyte anchoring helps overcoming the capillary interaction, due to the inter-particle liquid bridge while drying the sample, more effectively than for the same colloids dispersed in an aqueous solution. Under our experimental conditions, this experimental trick was found to control the capillary-induced aggregation down to a colloid surface-to-surface distance of nearly 40 nm for $D = 80$ nm [58].

Recently, the possibility of fabricating good quality short-range ordered metal nanohole distributions by our MNL-CL protocol (Fig. 1) was demonstrated [56] without a systematic study of the impact of using a polyelectrolyte monolayer on the ordering properties of the resulting colloidal distributions. The following sections present the physical guidelines applied to design our experiments and formulate a simple conceptual model to predict, on the basis of Coulomb repulsion strength, a threshold interparticle-spacing below which the influence of the polyelectrolyte monolayer on the mask may be observed and exploited in practice.

3.1. Deposition process of the polyelectrolyte monolayer

As overviewed in the introduction, the impact of the deposition time of a polyelectrolyte monolayer on the colloidal arrangement is not properly investigated in the literature.

To date, better colloidal mask was observed when using a triple polyelectrolyte layer rather than a PDDA monolayer obtained for an adsorption time as short as 30 s [31]. Typical reported PDDA adsorption time never exceeds 45 s [31,52-54]. Since the adsorption process of PDDA reaches 90% of saturation in 40 s [55], it is expected that unsaturated polyelectrolyte layer could impact negatively on the adsorption efficiency of the colloidal mask.

Besides the adsorption time, competing polymer chain-substrate electrostatic attraction and chain-chain electrostatic repulsion as well as chain conformation determine the charge distribution of the polyelectrolyte. Chain distribution can be characterized by two length-parameters: the average length of the adsorbed chains which depends on chain conformation (for instance, the contour length of a PDDA chain including 2000 monomers is 700 nm [60]) and the inter-chain spacing ($L_{ch\text{-}ch}$), dictated by the balance between chain-chain repulsion and chain-substrate attraction.

In our experiments, PDDA chains are expected to adsorb onto the oxygen plasma-processed substrate as an ultrathin laterally heterogeneous (i.e., forming a discrete chain distribution) monolayer, with degree of coverage/saturation depending on chain conformation and adsorption time Δt_{PDDA}. In turns, conformation and adsorption rates of the polyelectrolyte chains at the substrate-solution interface are sensitive to solution parameters, like salt type and content and polyelectrolyte concentration [41,61,62]. Salt-free polyelectrolyte solutions not only guarantee flat configuration of the adsorbed chains, due to unscreened intra-chain and inter-chain electrostatic repulsion, but also favor layer flatness by means of unscreened attractive substrate and saturated surface at a lower adsorbed amount [62]. Therefore, the absence of salt and a properly low PDDA concentration (0.2% in our experiments) [59] are optimal conditions for avoiding rough saturated films and conformational changes of the adsorbed PDDA chains. About Δt_{PDDA}, increasing its value from a minimum value of 40 s is expected to guarantee an effective adsorption-efficiency [41,55] and the possibility of investigating the interplay between Δt_{PDDA} and Δt_{PS} on the evolution of the colloidal mask.

3.2. Deposition process of colloids

Colloids adsorb and arrange onto a countercharged surface as a result of several processes: diffusion of the colloids from the bulk suspension to the collector surface, electrostatic anchoring of the colloids to the countercharged collector surface, repulsive interactions between adsorbed and flowing particles at the solid-liquid interface, repulsive interactions between the adsorbed particles, in-plane Brownian diffusion, and capillary lateral attractive forces pulling together the particles during drying [33,51,63]. Noteworthy, as the intensity of the attractive lateral capillary forces increases with the colloidal radius and the center-to-center distance between colloids, the influence of capillary forces is not significant in the case of small and well-separated particles. Depending of the ionic strength and concentration of the colloidal suspension, capillary forces may overcome the electrostatic interparticle repulsion during the drying procedure, leading to agglomeration effects [64].

Range of interparticle electrostatic interactions and zeta potential of the polyelectrolyte collector surface control final fractional coverage and ordering of the colloidal mask [51]. While the early stage of the colloid adsorption process is ruled by colloid-polyelectrolyte surface electrostatic attraction, upon increasing coverage repulsive interactions between already adsorbed and adsorbing colloids dominate and stabilize the colloidal distribution [65]. Hence, an adsorption attempt of a colloid onto a polyelectrolyte countercharged surface can be successful if locally the substrate attraction overcomes the repulsion from already adsorbed neighbor colloids. As a result, colloidal adsorption gets blocked when

the colloid-polyelectrolyte attraction is counterbalanced and overcome by the repulsion between adsorbing and already adsorbed beads.

When colloid-to-colloid spacing approaches the colloidal diameter, self-assembling is governed by interparticle electrostatic repulsion whereas attraction forces, due to capillary effects that occur during drying, pull particles together into aggregates.

3.3. Physical model to probe the impact of a polyelectrolyte monolayer on the formation of a colloidal mask

The characteristics of the distribution resulting from competition between the attractive potential of the polyelectrolyte and interparticle repulsion can be envisaged by comparing the decay length-scale of the inter-bead electrostatic repulsion ($L_{b\text{-}b}$) and the inter-chain spacing ($L_{ch\text{-}ch}$). To clarify this point, a laterally heterogeneous unsaturated polyelectrolyte layer with $L_{ch\text{-}ch} > L_{b\text{-}b}$ would lead to inhomogeneous colloidal mask with void regions in between the adsorbed colloids, where charge reversal is not achieved, independently on the range of interparticle repulsion. Differently, the condition $L_{ch\text{-}ch} < L_{b\text{-}b}$ would allow tuning coverage and order by increasing the adsorption time of both polyelectrolyte and mask, that is acting on the balance between interparticle repulsion and particle-collector surface attraction. Since the influence of the polyelectrolyte on the colloidal distribution would be obscured for $L_{b\text{-}b}$ much larger than $L_{ch\text{-}ch}$, decreasing L_{bb} (i.e., shortening the range of Coulomb interparticle repulsion) would lead to increased coverage by decreased threshold of blocking adsorption. Hence, $L_{b\text{-}b}$ acts as an upper limit, defining a regime where adsorbed colloids can act as effective markers of the polyelectrolyte adsorption efficiency on the basis of the competition between particle-polyelectrolyte attraction and interparticle repulsion.

Turning to colloids, the cornerstone of the actual understanding of the mechanisms of colloid adsorption onto a solid surface from bulk suspensions is the Deyaguin-Landau-Verwey-Overbeek (DLVO) theory [66,67] and its extension (termed XDLVO theory) including the Born repulsion term [68,69]. According to the DLVO model, the potential combines van der Waals attraction with double-layer electrostatic repulsion that is a volume exclusion (blocking) effect stemming from repulsive interactions between already adsorbed and trying to adsorb colloids. As in our case we deal with low concentration and salt-free colloidal suspensions, for our purpose it is appropriate to consider the DLVO potential dominated by the electrostatic repulsion.

In a simple model, given a colloidal bead, modelled by a sphere with charged surface Q and diameter D (Fig. 1(e)), dispersed in a salt-free aqueous suspension, the electrostatic potential at a radial distance r from the colloidal surface is given by $V(r) = k\,Q/r$. Simple mathematics enables to evaluate the distance L_b from the surface of a single bead at which its electrostatic potential falls off at 1/e (where $e = 2.71828$ is the Euler number) of the surface value V_0. Fulfilling the condition $V(r) = V_0/e$ yields the relationship

$$L_b = (e/2)D$$

According to the meaning of L_b, the electrostatic repulsion between two likely charged beads suspended in a salt-free solution can be considered effective when they are separated by surface-to-surface distance shorter than L_b (Fig. 1(e)), meaning a center to center distance shorter than the quantity L_{bb} defined as follows

$$L_{bb} = L_b + D$$

Since the saturated adsorption distribution of a colloidal mask is dominated by interparticle repulsion, this simple model can be applied to formulate a condition on $L_{b\text{-}b}$ (where $L_{b\text{-}b} > L_{ch\text{-}ch}$) enabling to exploit colloids as sensitive probes of the influence of the polyelectrolyte substrate on the adsorption process. That is, electrostatic repulsion between adsorbing PS nanospheres with diameter D_{PS} becomes active in affecting their relative positioning on a polyeletrolyte monolayer when $d_{NN} < L_{b\text{-}b} = L_b + D_{PS}$, where d_{NN} is the average (center to center) interparticle spacing. Experimentally, based on the relationship

$$L_{bb} = L_b + D_{PS}\left(L_b = (e/2)\,D_{PS}\right)$$

L_{bb} can be shortened by reducing D_{PS} and/or by salt addition (i.e., screened interparticle repulsion) to the colloidal suspension. Furthermore, the condition $d_{NN} < L_{b\text{-}b}$ can be experimentally verified by statistical analysis of the distribution.

The formulated model implies that any influence of the adsorption efficiency of the polyelectrolyte collector surface can be better disclosed for small colloidal diameter. Indeed, more flexible tuning of the colloid distribution and more extensive checking of the predictions of the developed electrostatic model will be demonstrated for $D_{PS} = 80$ nm rather than for $D_{PS} = 100$ nm. The underlying reason is that a shortened length-scale of the interparticle Coulomb repulsion also decreases L_{bb}, which causes the condition $d_{NN} < L_{bb}$ to be fulfilled for values of d_{NN} in the range of interest in applications (i.e., from several tens to hundreds of nanometers).

4. Results and discussion

On the basis of the presented physical principles underlying our experiments, we investigate the influence of the designed deposition conditions and their interplay on the distribution of our colloidal masks according to the flowchart reported in Fig. 2. For each considered set of experimental parameters (i.e. colloid diameter (D_{PS}), colloid concentration (C_{PS}), salt concentration (C_{NaCl}), deposition time of PDDA (Δt_{PDDA}) and PS colloids (Δt_{PS})), interparticle spacing d_{NN} was decreased down to its minimum value compatible with short-range ordering of the mask. Since shortening d_{NN} is associated with increasing fractional coverage, the adsorption efficiency of PDDA can be reliably checked at short Δt_{PS} for PS colloids getting closer and closer. Also, results are discussed by keeping in mind the threshold distances defined within the framework of simple electrostatic model introduced above. Therefore, on one hand, experimental evidence is a test of the reliability of the simple electrostatic model and, on the other hand, the simple electrostatic model is applied for designing experiments. As it will be demonstrated and discussed, both approaches are consistent.

4.1. PDDA polyelectrolyte monolayer

In order to inspect the surface morphology of the PDDA monolayer deposited for $\Delta t_{PDDA} = 40$ s, 1 min, 2 min, 5 min, SEM plan view images were acquired. Similar morphologies were observed regardless of the deposition time. In this respect, Fig. 3 shows the low (Fig. 3(a)) and high (Fig. 3(b)) magnification images of the PDDA film deposited for $\Delta t_{PDDA} = 2$ min, as representative of the morphology obtained for varying Δt_{PDDA}. The layer is very smooth, as suggested by the absence of topographic contrast at the two very different imaged length scale, despite the experimental conditions (50° sample tilt angle and accelerating voltage as low as 2 kV) used to enhance this kind of contrast. Spare topographic details, visible in the low and high magnification images and used for the fine adjustment of the electro-optical imaging conditions, point out, by comparison, the flat topography of the deposited PDDA monolayer. This result was expected on the basis of the experimental conditions set for preparing the PDDA solution, namely salt-free and low PDDA concentration solution, both favoring an extended and flat (or rod-like) conformation of the adsorbed chains, due to the electrostatically repelling identically charged groups along the same chain [59,70]. The demonstrated absence of topographic features, like chain agglomeration or voids formation, for all the PDDA deposition times, rules out any influence of the PDDA topography on the arrangement of the overlying colloidal mask. Hence, any impact of the PDDA monolayer on the formation of the colloidal mask would depend on the degree of adsorption saturation/ binding efficiency resulting from Δt_{PDDA} [51].

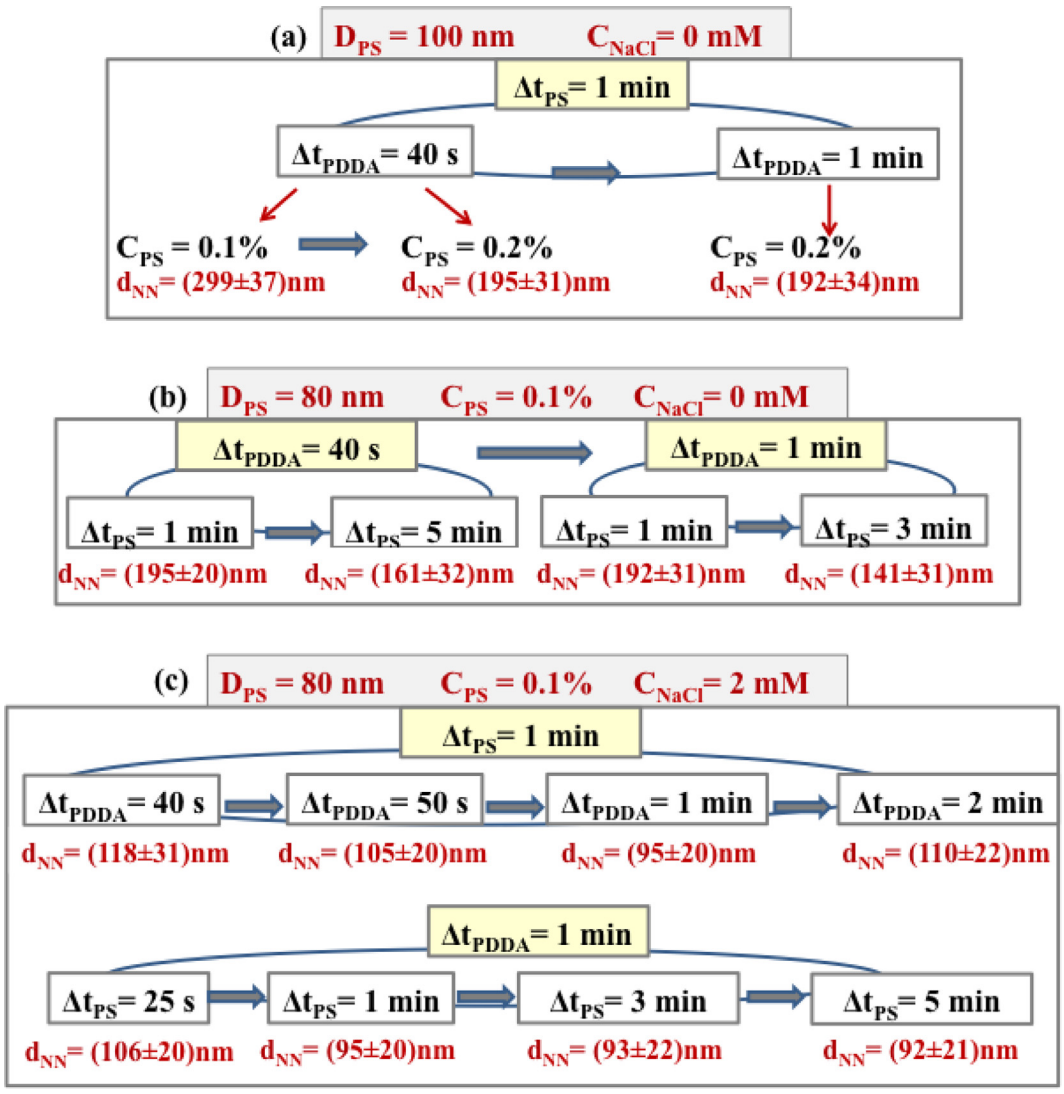

Fig. 2. (Color online) Flowchart overviewing the performed experiments reporting the changes of the experimental parameters planned to decrease the interparticle spacing d_{NN} down to its minimum value compatible with short-range ordering of the colloidal mask. Panel (a) refers to salt-free colloidal suspensions with D_{PS} = 100 nm. Panel (b) refers to D_{PS} = 80 nm, C_{PS} = 0.1% and C_{NaCl}= 0 mM. Panel (c) refers to D_{PS} = 80 nm, C_{PS} = 0.1% and C_{NaCl}= 2 mM. In any case the applied changes of Δt_{PDDA} and Δt_{PS} are shown along with the resulting value of d_{NN}. Arrows indicate an increasing value of the quantity under consideration.

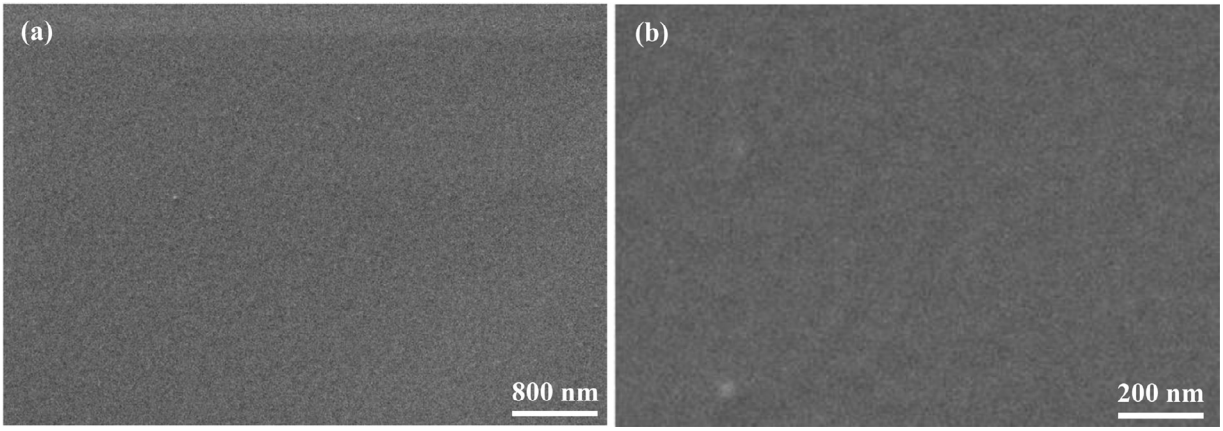

Fig. 3. (a) Low and (b) high magnification SEM images of a PDDA monolayer deposited for Δt_{PDDA}= 2 min acquired under 50° sample tilt angle and for an accelerating voltage as low as 2 kV.

Table 2
Interparticle spacing (d_{NN}) and fractional coverage (cvg) of colloidal masks fabricated by the MNL-CL protocol using colloids with diameter D_{PS}= 100 nm. The quantities L_b and L_{bb} are decay length-scales of electrostatic repulsion defined as L_b=(e/2) D_{PS} and L_{bb}= L_b+ D_{PS}.

D_{PS}=100 nm / L_b(100)~136 nm / L_{bb}(100)~236 nm			
Sample	d_{NN} (nm)	cvg (%)	Model
PS(40s-1 min,0.1%,100 nm)	299±37	9.3 ± 0.6	d_{NN} > **L_{bb}(100)**
PS(40s-1 min,0.2%,100 nm)	195±31	20±1	d_{NN}
PS(1min-1 min,0.2%,100 nm)	192±34	19±1	< **L_{bb}(100)**

Table 3
Interparticle spacing (d_{NN}) and fractional coverage (cvg) of colloidal masks fabricated by the MNL-CL protocol using colloids with diameter D_{PS}= 80 nm. The quantities L_b and L_{bb} are decay length-scales of electrostatic repulsion defined as L_b=(e/2) D_{PS} and L_{bb}= L_b+ D_{PS}.

D_{PS} = 80 nm / L_b(80)~109 nm / L_{bb}(80)~189 nm			
Sample	d_{NN} (nm)	cvg (%)	Model
PS(40s-1 min,0.1%,80 nm)	200±20	8.7 ± 0.5	d_{NN}
PS(1min-1 min,0.1%,80 nm)	192±31	9.1 ± 0.6	>
PS(40s-5 min,0.1%,80 nm)	161±32	13.7 ± 0.8	**L_{bb}**
PS(1min-3 min,0.1%,80 nm)	141±31	18±1	**(80)**
PS(2min-1 min,0.1%,80 nm)	110±22	26±2	**L_{bb}**
PS_{NaCl}(40s-1 min,0.1%,80 nm)	118±31	11.4 ± 0.7	**(80)**
PS_{NaCl}(50s-1 min,0.1%,80 nm)	105±20	25±1	
PS_{NaCl}(1min-25 s,0.1%,80 nm)	106±20	29±2	
PS_{NaCl}(1min-1 min,0.1%,80 nm)	95±21	31±2	
PS_{NaCl}(1min-3 min,0.1%,80 nm)	93±22	32±2	
PS_{NaCl}(1min-5 min,0.1%,80 nm)	92±21	33±2	
PS_{NaCl}(2min-1 min,0.1%,80 nm)	110±22	26±2	

4.2. Impact of the PDDA monolayer on the colloidal distribution

According to the above discussion, the impact of PDDA coverage/potential on the colloid distribution is expected to be observable for d_{NN}< L_{bb}, where L_{bb}= L_b+ D_{PS}. The values of L_{bb} corresponding to the values of D_{PS} under consideration are L_{bb}(80) ~ 189 nm (associated with D_{PS}=80 nm and L_b(80) ~ 109 nm) and L_{bb} (100) ~ 236 nm (associated with D_{PS}=100 nm and L_b(100) ~ 136 nm). Aiming at shortening d_{NN} below the above reported L_{bb} values, several preliminary control experiments were performed by varying the fractional coverage of the colloidal distribution (Fig. 2, Tables 2 and 3).

Fig. 4 shows plan-view SEM images of the colloidal distributions adsorbed onto a PDDA monolayer by varying: Δt_{PDDA} (i.e., Δt_{PDDA}=40 s, 1 min), Δt_{PS} (i.e., Δt_{PS}=40 s, 1 min, 5 min), the colloidal diameter (i.e., D_{PS}=80 nm, 100 nm) and the concentration (i.e., C_{PS}= 0.1%, 0.2%) of the salt-free colloidal suspension. The interparticle spacing evaluated by SEM images is listed in the bottom left panel of Fig. 4.

4.2.1. Colloidal distributions associated with D_{PS}=100 nm and salt-free suspensions

For D_{PS}=100 nm, the statistical analysis of SEM plan-view images in Figs. 4(a)-(c) yielded the values of d_{NN} listed in Table 2, that is (299±37) nm for PS(40s-1 min,0.1%,100 nm), (195±31) nm for PS(40s-1 min,0.2%,100 nm) and (192±34) nm for PS(1min-1 min,0.2%,100 nm).

Since L_{bb}(100)=236 nm, the condition d_{NN}<L_{bb}(100) is fulfilled for the last two samples, by increasing C_{PS} from 0.1 to 0.2%, leading to comparable d_{NN} and cvg. Therefore, Δt_{PDDA} prolonged from 40 s to 1 min can only affect the PS nanosphere distribution.

As matter of facts, at the lowest coverage, a uniform arrangement with quite negligible agglomeration is observed, whereas, for increasing coverage the presence of faint agglomeration is detected.

Notably, PS(1min-1 min,0.2%,100 nm) (Fig. 4(c)) exhibits reduced agglomeration (18 dimers, 6 trimers, 1 agglomerate with more than 3 PS nanospheres are detected in the imaged area) with respect to PS(40s-1 min,0.2%,100 nm) (Fig. 4(b)) (16 dimers, 9 trimers, 6 agglomerates with more than 3 PS nanospheres). These differences point out an impact of the PDDA underlayer on the colloid arrangement.

In general, formation of agglomerates may result from capillary forces becoming more and more active for interparticle spacing approaching the particle diameter. Under these conditions favoured by drying, lateral capillary attraction may exceed the interparticle Coulomb repulsion.

As d_{NN} > D_{PS} in the case of the set of samples under consideration, capillary forces are expected to have poor impact. Therefore, the reduced agglomeration of PS(1min-1 min,0.2%,100 nm) compared to PS(40s-1 min,0.2%,100 nm) points out the impact of the improved adsorption efficiency (increased attractive surface potential) resulting from a longer Δt_{PDDA} that favors on-site colloidal anchorage with limited rearrangements by in-plane Brownian diffusion [51].

Definitively, as both PS(40s-1 min,0.2%,100 nm) and PS(1min-1 min,0.2%,100 nm) fulfill the condition d_{NN} < L_{bb}(100) ~236 nm, the differences observed in their distributions are also consistent with the prediction of our simple interpretative model.

4.2.2. Colloidal distributions associated with salt-free suspensions

For D_{PS}=80 nm, Figs 4(d)-(g) show SEM plan-view images of the samples prepared by setting C_{PS} = 0.1% and Δt_{PDDA}= 40 s, 1 min. Notably, C_{PS}= 0.2% was not considered because shorter-ranged Coulomb repulsion associated with smaller D_{PS} would favor agglomeration effects, thus limiting the possibility to effectively decrease d_{NN} over a wide range of values by increasing Δt_{PS}.

Furthermore, in practice, increasing the coverage by tuning Δt_{PS} is a simpler strategy than varying the solution concentration. As a result of statistical analysis, d_{NN} was measured to be (200±20) nm for PS(40s-1 min,0.1%,80 nm) and (192±31) nm for PS(1min-1 min,0.1%,80 nm) (Table 2). Since Δt_{PS} = 1 min in both cases, the increased coverage is consistent with the expected improved adsorption efficiency resulting from longer Δt_{PDDA} [51].

In regard to the mask distribution, the two samples are very similar and exhibit well separated PS nanospheres, with the rare presence, in the case of longer Δt_{PDDA}, of small agglomerates that can be responsible of the increased dispersion of d_{NN}.

A few comments are worth about D_{PS}=80 nm as compared to D_{PS}=100 nm.

First, PS(40s-1 min, 0.1%,100 nm) (Fig. 4(a)) and PS(40s-1 min, 0.1%,80 nm) (Fig. 4(d)) present similar arrangements (well isolated particles and rare formation of dimers) with decreased d_{NN} from (299±37) nm to (202±20) nm. The underlying physical reason is that the interparticle spacing rescales with the bead diameter and related surface charge, given that the decay length of interparticle Coulomb repulsion affects the relative positioning of the adsorbed colloids. In this sense, the MNL-CL protocol is repeatable as a function of the colloidal size.

Second, the identical interparticle spacing of PS(1min-1 min,0.2%,100 nm) and PS(1min-1 min,0.1%,80 nm) (Tables 2 and 3) achieved despite the stronger Coulomb repulsion associated with larger D_{PS} points out that the concentration of the colloidal solution may be an effective parameter for increasing coverage under short-time adsorption. Instead, for D_{PS}=80 nm, clustering was found to be more difficult to control for increasing Δt_{PS} if C_{PS}=0.2% whereas C_{PS} < 0.1% wt required unpractical prolonged Δt_{PS} to achieve a comparable coverage. Hence, colloidal concentration and adsorption time can be, in principle, exploited to tailor the fractional coverage, but the impact of the decay-range of interparticle repulsion and capillary forces also needs to be ascertained by preliminary experiments.

Third, the differences observed in the colloidal distribution of PS(40s-1 min,0.2%,100 nm) (Fig. 4(b)) versus PS(1min-1 min,0.2%,100 nm) (Fig. 4(c)) i.e. enhanced clustering at Δt_{PDDA}= 40 s, do not occur in the case of PS(40s-1 min,0.1%,80 nm) (Fig. 4(d)) as compared to PS(1min-1 min,0.1%,80 nm) (Fig 4(e)), that are very similar. Since the attractive bead-PDDA interaction is stronger for

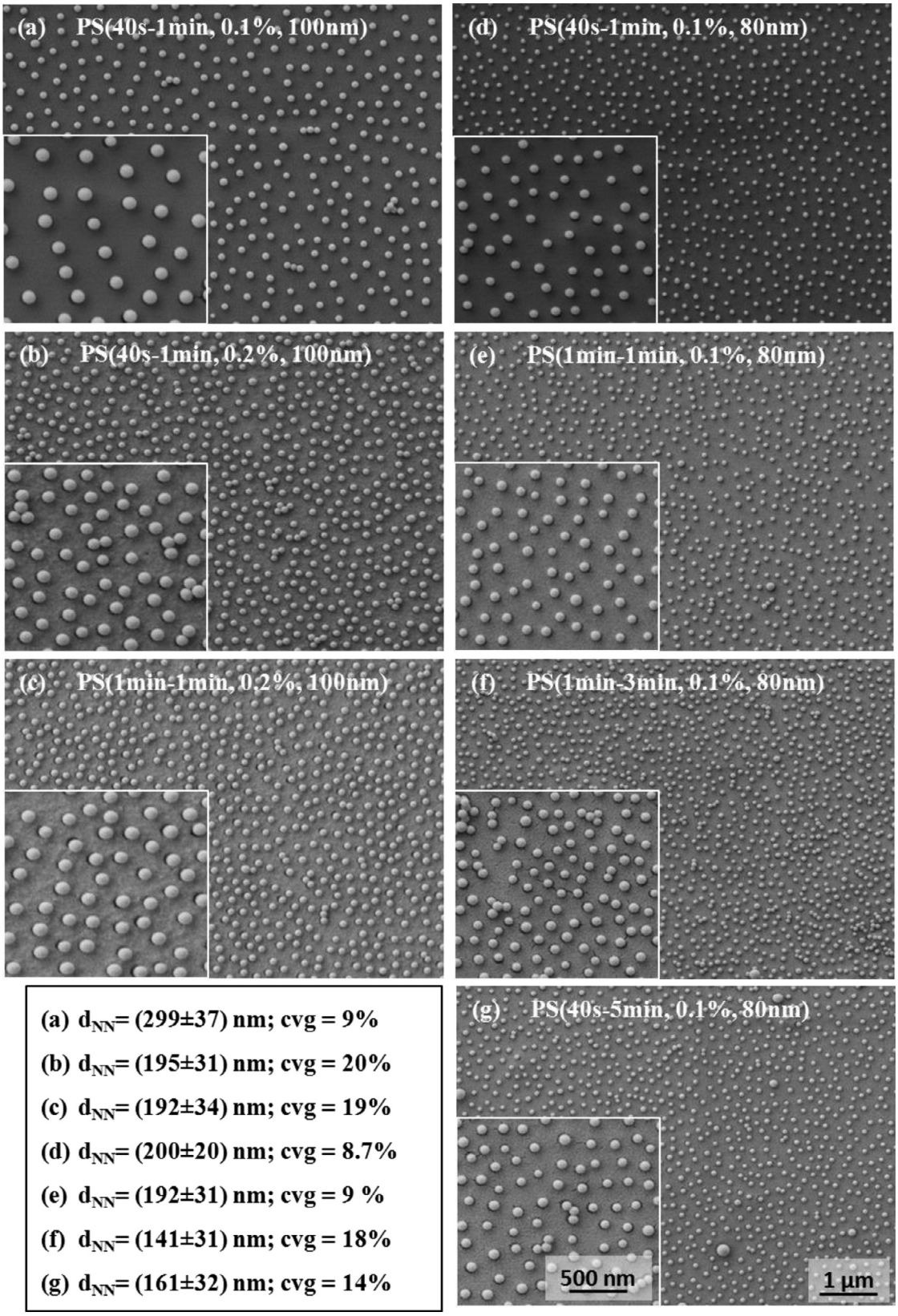

Fig. 4. Plan-view SEM images of the colloidal distributions adsorbed onto a PDDA monolayer under the conditions Δt_{PDDA}=40 s, 1 min, Δt_{PS}=40 s, 1 min, 5 min, D_{PS}=80, 100 nm and C_{PS}= 0.1, 0.2%. The interparticle spacing (d_{NN}) and the corresponding coverage (cvg) evaluated by SEM images are listed in the bottom left panel.

D_{PS}=100 nm than for D_{PS}=80 nm, the occurrence of clustering in PS(40s-1 min,0.2%,100 nm) would indicate a not effective adsorption efficiency from the collector surface able to avoid surface rearrangements driven by Brownian diffusion and interparticle Coulomb repulsion for short-time adsorption. As a confirmation, turning from Δt_{PDDA}= 40 s to Δt_{PDDA}= 1 min while keeping Δt_{PS}= 1 min, the improved adsorption efficiency of the polyelectrolyte collector surface becomes effective in limiting surface rearrangements ruled by capillary forces.

For D_{PS}=80 nm, similar behavior is not observed because, despite the weaker colloid-PDDA attraction, capillary forces are less impacting on the arrangement of closely-spaced colloids.

The balance between PDDA adsorption efficiency, interparticle repulsion and capillary forces is also confirmed by the saturated adsorption condition for Δt_{PDDA}= 40 s and Δt_{PDDA}= 1 min that was achieved, respectively, for Δt_{PS}=5 min (sample PS(40s-5 min,0.1%,80 nm) in Fig 4(f) with d_{NN}=(161±32)) and Δt_{PS}=3 min (sample PS(1min-3 min,0.1%,80 nm) in Fig 4(g) with d_{NN}=(141±31) nm) (Table 3). The distribution of PS(40s-5 min,0.1%,80 nm) exhibits a uniform coverage and local agglomerates are visible, generally consisting of short chains involving few units (dimers and trimers). For PS(1min-3 min,0.1%,80 nm), a more effective increase in the coverage can be observed with formation of sparse clusters, absent in the case of PS(40s-5 min,0.1%,80 nm). In practice, coverage estimations indicate that a slight increase of Δt_{PDDA} improves the coverage more effectively than Δt_{PS} lasting a few minutes. The physical mechanism is that, for short time adsorption Δt_{PS}, meaning low coverage, the dominance of the PDDA-colloid attractive interaction over the interparticle repulsion at the solution-PDDA interface causes the adsorption efficiency to depend mainly on Δt_{PDDA}. Once Δt_{PDDA} is optimized, increasing Δt_{PS} exploits the interplay between colloid-PDDA attraction and colloid-colloid repulsion to drive electrostatically stabilized ordering

In conclusion, we provided evidence that the PDDA collector surface plays a role in tuning the binding efficiency of colloids and influences the colloidal arrangement, if sufficiently long adsorption time Δt_{PDDA}, generally larger than the ones commonly reported in the literature [31,52-55] is used. On the other hand, Δt_{PDDA}= 1 min, rather than prolonged to a few minutes, was demonstrated to be enough to provide effective adsorption efficiency, being the distribution further tunable by varying Δt_{PS}. Therefore, the impact of PDDA consists of two effects: i) adsorption efficiency of the colloidal solution, that can be straightforwardly observed for increasing Δt_{PDDA} combined with short-time adsorption of the colloids, and ii) ordering of the mask that depends on the net balance between the active interactions.

4.2.3. Colloidal distributions associated with salt-added suspensions

The observed differences between PS(40s-5 min,0.1%,80 nm) and PS(1min-3 min,0.1%,80 nm), both fulfilling the condition $d_{NN}<L_{bb}(80)\sim189$ nm, might be due to increased coverage rather than to the PDDA collector surface. Hence, in order to validate our model, colloidal distributions with the same further increased coverage and deposited for Δt_{PDDA}= 40 s and Δt_{PDDA}= 1 min have to be compared. Since PS(40s-5 min,0.1%,80 nm) and PS(1min-3 min,0.1%,80 nm) correspond to saturated adsorption, further shortening of d_{NN} may not be obtained by salt-free colloidal solutions. In turn, using salt-added colloidal suspension allows one to shorten d_{NN} due to shortened-ranged colloid-colloid electrostatic repulsion. In experiments discussed hereafter C_{NaCl}=2 mM, which is to be intended as an upper value of ionic strength allowing us to decrease d_{NN} in such a way to satisfy the constraint $d_{NN}<L_{bb}$. Preliminary salt-added experiments demonstrated that C_{NaCl}=2 mM is a trade-off value which, from one side, prevents clustering, severely observed for C_{NaCl} >2 mM, and, from the other side, allows one a tuning of coverage over a reasonable range, not achievable for C_{NaCl} < 2 mM [56].

Hence, hereafter, samples deposited from electrostatically screened (C_{NaCl} = 2 mM) colloidal suspensions of PS nanospheres with D_{PS}=80 nm and C_{PS}= 0.1% will be presented and discussed (see the panel (c) of the flowchart in Fig. 2). For calibration purposes and according to the results presented in the case of salt-free colloidal suspensions, we considered Δt_{PDDA}= 40 s as a starting value and studied the effects of increasing it progressively (50 s, 1 min, 2 min) (Figs 5 and 6).

Plan-view SEM image of NH_{NaCl}(40s-1 min,0.1%,80 nm) (Fig 5(a)), that perfectly matches the distribution of the template colloidal mask PS_{NaCl}(40s-1 min,0.1%,80 nm) (Fig. 1), shows the presence of extended empty areas and locally disordered particle arraying. Statistical analysis yielded an interparticle spacing of d_{NN}=(118±31) nm (i.e., cvg=(11.4 ± 0.7)%), which is shorter than L_{bb}(80) (Table 3).

By comparison with the counterpart salt-free sample (PS(40s-1 min,0.1%,80 nm), Fig 4(d)), two main salt-related effects on distribution and degree of ordering of the mask have to be accounted for. First, salt-induced screening of the attractive colloid-PDDA interaction can reduce the adsorption efficiency of PDDA surface. Second, weakened interparticle electrostatic repulsion is not able to improve the level of ordering as far as colloids are far apart, as it occurs for short-time adsorption. Further control experiments were performed by increasing Δt_{PS} and Δt_{PDDA} independently. Given Δt_{PDDA}= 40 s, Δt_{PS} prolonged up to 10 min was found to induce no effective improvement of the homogeneity of the mask distribution due to the persistence of void areas and agglomeration effects that were the more enhanced the more prolonged Δt_{PS} was. Hence, Δt_{PDDA}= 40 s was demonstrated to be unsuitable for the purposes of our study.

For Δt_{PDDA}=50 s, plan-view SEM image of NH_{NaCl}(50s-1 min,0.1%,80 nm) is reported in Fig 5(b). As compared to NH_{NaCl}(40s-1 min,0.1%,80 nm), this sample exhibits reduced presence of voids and improved coverage leading to the statistical estimation d_{NN}= (105±20) nm (i.e., cvg=(25 ± 2)%). This result is consistent with the expected improved adsorption efficiency favoured by prolonging Δt_{PDDA}. The sample shows small agglomerates, favoured by increased coverage, and chain-like alignment of the particles. The same interparticle spacing as NH_{NaCl}(50s-1 min,0.1%,80 nm) was obtained by combining Δt_{PDDA}=1 min and Δt_{PS} =25 s (i.e., PS_{NaCl}(1min-25 s,0.1%,80 nm) in Fig. 6(a)) that was found to yield d_{NN}=(106±20) nm, corresponding to cvg=(29±2)%. The possibility of achieving the same coverage at a shorter deposition time Δt_{PS} clearly demonstrates the effective influence of Δt_{PDDA} on the ordering of the mask combined with improved adsorption efficiency [51]. Being $d_{NN}\sim106$ nm < L_{bb}(80), this evidence is also consistent with the expectations of our model.

For Δt_{PDDA}=1 min, the impact of Δt_{PS} increased from 25 s to 5 min can be observed by the corresponding series of samples shown in Figs 6(a)-(d). Statistical analysis of the SEM images under consideration provided the values of the interparticle spacing d_{NN} listed in Table 3: d_{NN}=(106±20) nm for PS_{NaCl}(1min-25 s,0.1%,80 nm), d_{NN}=(95±21) nm for PS_{NaCl}(1min-1 min,0.1%,80 nm), d_{NN}=(93 ± 22) nm for PS_{NaCl}(1min-3 min,0.1%,80 nm) and d_{NN}=(92 ± 21) nm for PS_{NaCl}(1min-5 min,0.1%,80 nm). The saturation adsorption coverage was achieved for Δt_{PS}= 1 min (sample PS_{NaCl}(1min-1 min,0.1%,80 nm) with d_{NN}=(93 ± 22) nm). All samples show a high density of PS nanospheres with increasing density and size of the agglomerates related to prolonging Δt_{PS} that can be ascribed to the attractive lateral capillary forces [63]. Depleted areas, mainly occurring close to the agglomerates, also form, depending on Δt_{PS}. Further control experiments demonstrated that increasing Δt_{PS} up to 12 min provides severe clustering effects with almost absent isolated colloids and systematic formation of voids in between the agglomerates. Therefore, under our experimental conditions, for Δt_{PDDA}=1 min, the adsorption efficiency of the PDDA collector surface being improved with respect to Δt_{PDDA}= 40 s, the saturation adsorption of colloids is quickly achieved at short-time adsorption (Δt_{PS}=1 min). Further prolonging Δt_{PS} is detrimental for capillary-induced clustering effects, that deteriorate the distribution and obscure the interplay between the adsorption times Δt_{PDDA} and Δt_{PS}, rather than enabling an effective improvement of the coverage.

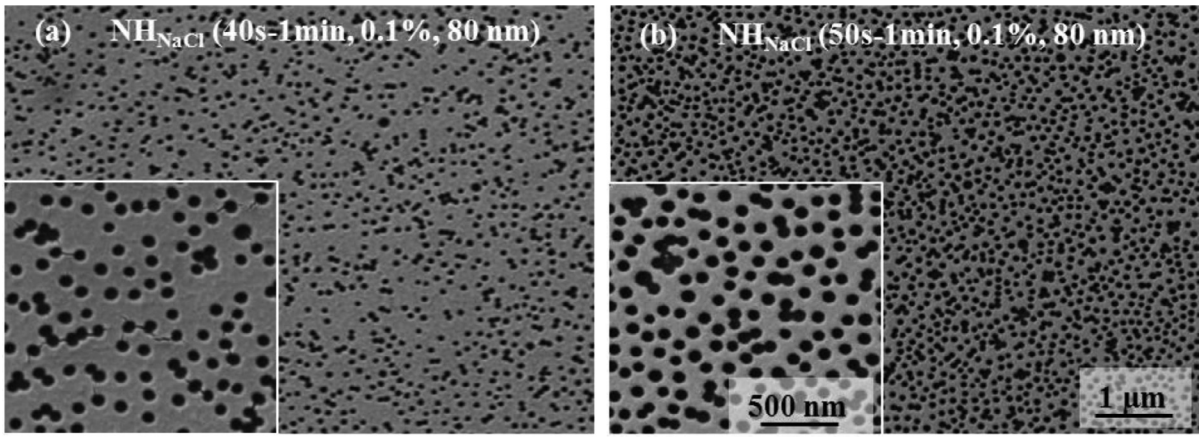

Fig. 5. Plan view SEM images of the nanohole distributions associated with the colloidal masks (a) PS_{NaCl} (40s-1 min, 0.1%, 80 nm) and (b) PS_{NaCl} (50s-1 min, 0.1%, 80 nm).

On comparing Δt_{PDDA}=1 min with Δt_{PDDA}=2 min, SEM images of PS_{NaCl}(2min-1 min,0.1%,80 nm) (Fig. 6(e)) and PS_{NaCl}(1min-1 min,0.1%,80 nm) (Fig. 6(b)) demonstrate for Δt_{PDDA}= 2 min a more inhomogeneous distribution with evident agglomeration effects, due to capillary interactions favoured by high coverage (d_{NN}=(110±22) nm and cvg=(26±2)%). Agglomeration is responsible of the seemingly increased d_{NN} with respect to d_{NN}=(95±21) nm of PS_{NaCl}(1min-1 min,0.1%,80 nm). The provided experimental evidence indicates that, in practice, Δt_{PDDA}= 1 min could be a better condition than Δt_{PDDA}= 2 min because the high adsorption efficiency given by increased Δt_{PDDA} does not allow to exploit an increase of Δt_{PS} for tuning coverage and ordering without the detrimental contribution from capillary interactions. Definitively, Δt_{PDDA} impacts on the characteristics of the distribution depending on the coverage tuned by Δt_{PS}.

4.3. Ordering degree of the colloidal mask and applicative implications

The interplay between Δt_{PDDA} and Δt_{PS}, with and without electrostatic screening, was also studied from the point of view of the correlated disorder of the colloidal masks, resulting from the application of the MNL-CL protocol. This was achieved by a quantitative method, based on mathematical image processing tools (i.e., "image autocorrelation" and "Fast Fourier Transform") applied to selected areas of SEM micrographs. The method allowed: i) to discover local periodic structures, difficult to be observed due to their very short-range order, and ii) to derive and measure a length-scale parameter, working as the equivalent of the lattice parameter characteristic of ideally ordered colloidal arrangements [56].

Fig. 7 compares the results of the investigation of colloidal masks deposited for Δt_{PDDA} increased from 1 to 2 min (i.e., saturated adsorption for the PDDA monolayer) and Δt_{PS} prolonged from 25 s to 3 min (i.e., from unsaturated to saturated colloidal adsorption, where the highest degree of correlated disorder occurs), in the presence (Figs. 4(a)-(c)) and in the absence (Figs. 4(d)-(f)) of salt.

For each mask, the region of interest is reported together with its autocorrelation image and the intensity profiles of the FFTs along a line passing through the center to show the occurring of eventual maxima. The FFT of the autocorrelation image was able to reveal the eventual presence of intensity maxima, corresponding to the presence of periodicity in the image, and to determine the relevant periodicity length. It is worth noticing that, without electrostatic screening, the colloidal arrangement is able to evolve towards a short range ordered distribution, whose order is not deteriorated by the coverage increase and whose periodicity length decreases with the increase of the coverage. In particular, under salt-free conditions and Δt_{PDDA}= 1 min, by increasing Δt_{PS} from 1 min (Fig. 7(a)) to the saturation threshold (Δt_{PS}=3 min, Fig. 7(b)), the intensity profiles of the FFTs show the presence of similar maxima, corresponding to periodicity length of (170±10) nm and (155±8) nm, respectively. For Δt_{PS} = 1 min, by doubling Δt_{PDDA} from 1 min to 2 min, the intensity maxima in the FFTs yield periodicity length decreasing from (170±10) nm to (130±8) nm (Fig. 7(c)). The obtained estimations of the periodicity length are consistent, within the experimental uncertainty, with the statistical values of d_{NN} reported in Table 3. Hence, under salt-free conditions, our analysis demonstrates quantitatively the occurrence of correlated disorder. Salt-related screened repulsion causes a rapid evolution of the colloid distribution towards a total loss of order that is present only for very low Δt_{PS} (i.e., 25 s, Fig. 7(d)), as it can be observed by the FFT analyses reported in Figs. 7(d)-(f).

Definitively, two main conclusions result from the correlated disorder analysis. First, autocorrelation and FFT analyses demonstrate a method to eventually associate a periodicity-like length to short-range ordered colloid distributions that, in principle, is a rigorous way of ascertaining the occurrence of correlated disorder. Second, on comparing salt-free with salt-related situations, we were able to extend the results of our previous studies [56] and demonstrate that in the presence of salt it is not possible to efficiently exploit the interplay between Δt_{PDDA} and Δt_{PS} to control a colloid distribution in terms of order and homogeneity.

An important applicative issue of the above discussion is reported in Fig. 8 that shows the transmittance spectra of gold nanohole samples fabricated by using salt-free (i.e., NH(40s-5 min), NH(1min-1 min), NH(1min-3 min) and NH(2min-1 min) in Fig 8(a)) and salt-added (i.e., NH_{NaCl}(1min-25 s) and NH_{NaCl}(1min-1 min) in Fig 8(b)) PS nanosphere suspensions according to the experimental protocol sketched in Fig. 1. A detailed identification of the spectral features of such nanohole arrangements is reported elsewhere [56].

Noteworthy, on comparing NH(1min-1 min) and NH_{NaCl}(1min-1 min) (and NH_{NaCl}(1min-25 s)), it is evident that salt-related disordering effects (confirmed by the autocorrelation analysis) cause flattening/loss of the transmission resonances occurring in the case of the samples deposited using salt-free suspensions [56]. In principle, since in perforated plasmonic metal arrays correlated disorder is demanding to observe peculiar electric field enhancement (transmission resonances) [18,71], transmission resonances are characteristic of the presence of short-range ordering hole-to-hole correlation and are affected by changes in the degree of ordering [72].

The sensing performances, in terms of response to changes of the surrounding refractive index, of NH(40s-5 min), NH(1min-3 min) and NH(2min-1 min), corresponding to the saturated adsorption colloidal masks prepared for Δt_{PDDA}=40 s (sample PS(40s-5 min,0.1%,80 nm)), Δt_{PDDA}= 1 min (sample PS(1min-3 min,0.1%,80 nm)) and Δt_{PDDA}= 2 min (sample PS(2min-1 min,0.1%,80 nm)), were estimated to be (349±39) nm/RIU, (296±32) nm/RIU and (230±30) nm/RIU, respec-

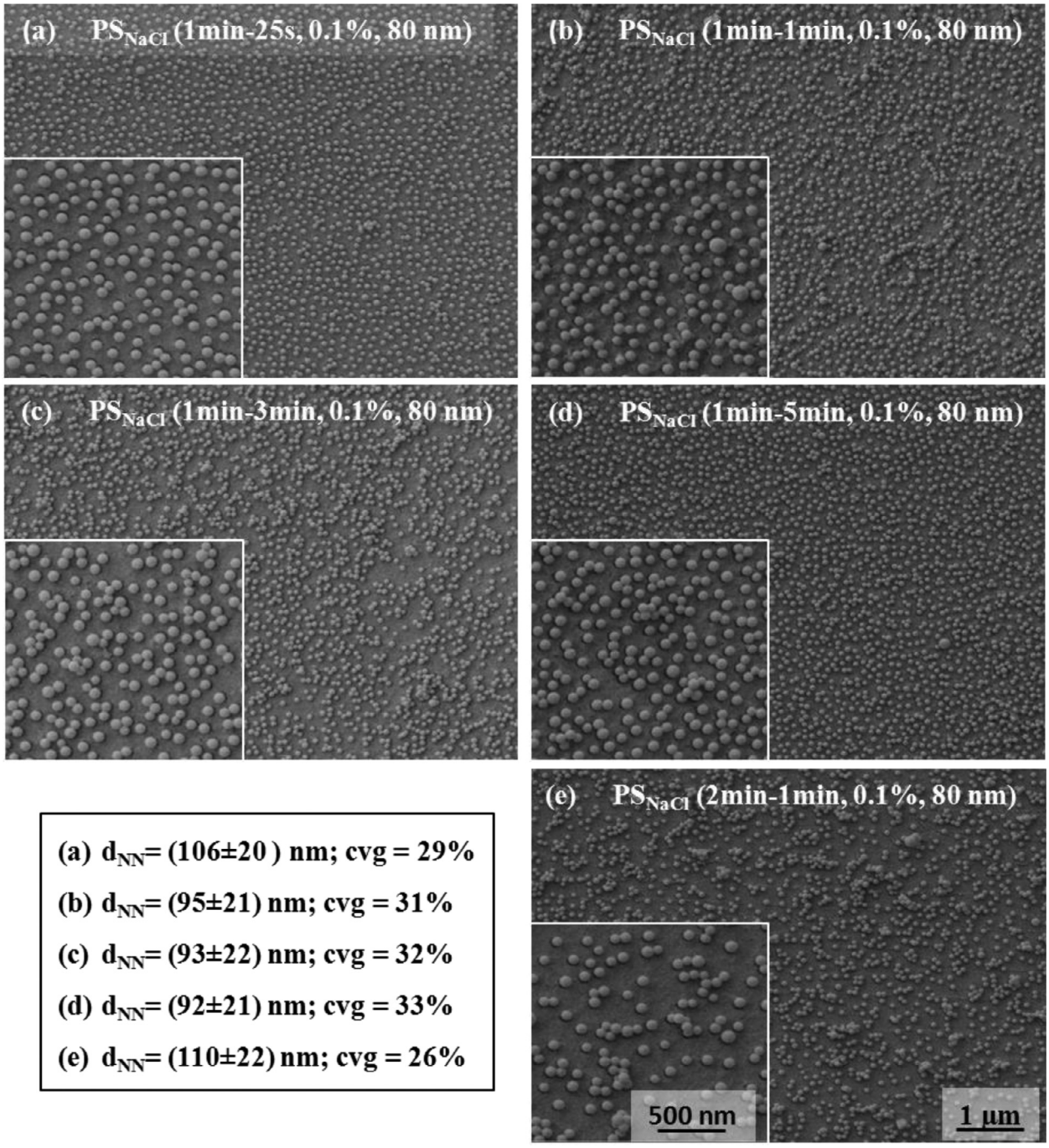

Fig. 6. Plan-view SEM images of the colloidal distributions adsorbed onto a PDDA monolayer under the conditions Δt_{PDDA}=1 min, 2 min, Δt_{PS} = 25 s to, 1 min, 3 min,5 min, D_{PS}=80 nm, C_{PS}= 0.1 and C_{NaCl}= 2 mM. The interparticle spacing (d_{NN}) and the corresponding coverage (cvg), evaluated by statistical tools based on SEM images, are listed in the bottom left panel.

tively. The highest measured value is comparable with or even better than other reports (see Ref [56] and references therein). More details about the sensing measurements, that are beyond the scope of the present paper, can be found elsewhere [56].

4.4. Concluding remarks: application guidance and potentialities of the mnl-cl protocol

Going beyond the set-up of a new protocol presented elsewhere [56], herein a systematic study was presented of the effect of the critical deposition parameters on the colloidal distributions, with the support of a simple interpretative model.

In order to discuss generality, conceptual implications and useful practical guidance of the MNL-CL protocol, a few remarks are mandatory.

i) Our experiments and the relevant comprehensive discussion demonstrate that the MNL-CL protocol works if properly applied, meaning that it overcomes successfully the limitations of the mentioned literature based on single polyelectrolyte layer. Our research demonstrates the physical consistency of our results with the accepted basic knowledge on colloidal self-assembly and the reproducibility of the MNL-CL protocol.

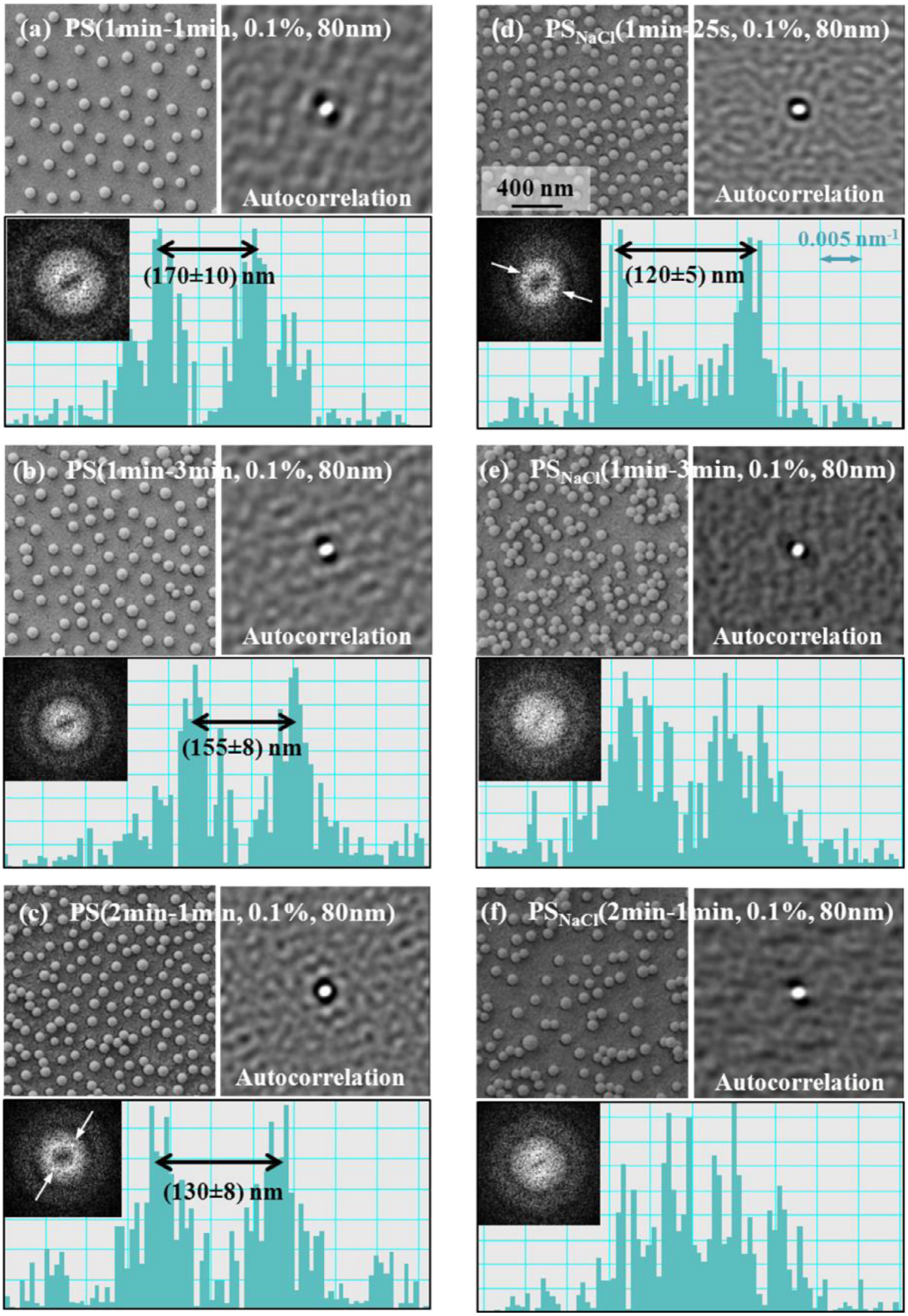

Fig. 7. (Color online) FFT of the autocorrelation images calculated by SEM images of the colloidal masks obtained with Δt_{PDDA} increasing from 1 to 2 min and Δt_{PS} increasing from 25 s to 3 min, (a)-(c) with and (d)-(f) without salt. For each mask, the region of interest is reported together with its autocorrelation image and the intensity profiles of the FFTs along a line passing through the center to show the eventual presence of intensity maxima corresponding to an ordering length-scale.

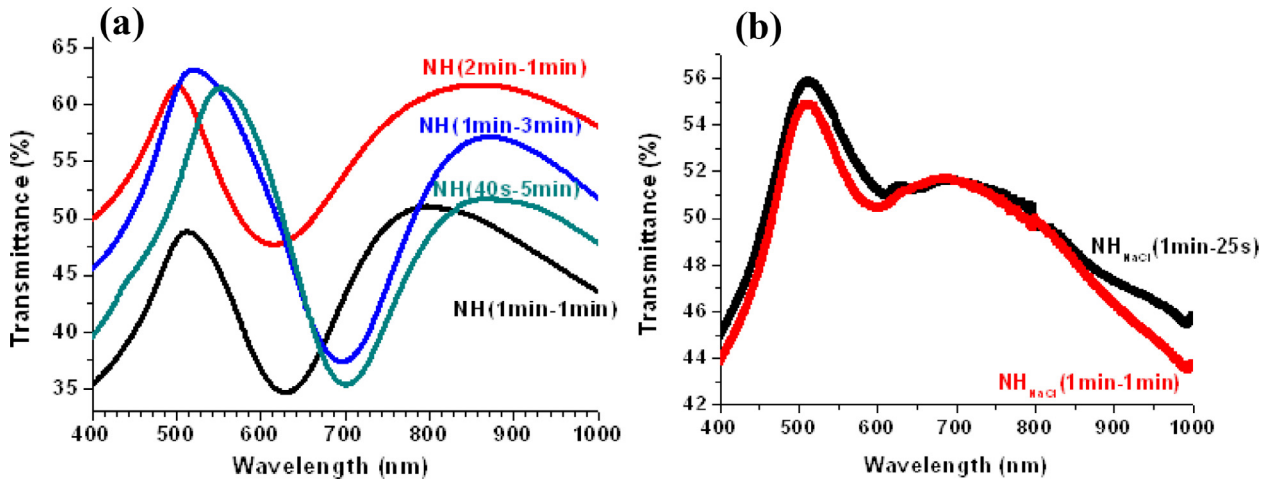

Fig. 8. (Color online) Transmittance spectra of gold nanohole systems fabricated based on the colloid mask templates deposited by the MNL-CL protocol given by: (a) salt-free (PS(2min-1 min), PS(1min-3 min) and PS(1min-1 min)) and (b) salt-added (PS(1min-25 s), PS(1min-50 s)) polystyrene nanosphere suspensions. The curves are identified by the nomenclature introduced in the experimental paragraph.

ii) As comprehensively demonstrated, spacing (d_{NN}) and ordering of a colloidal mask fabricated by the MNL-CL protocol are dictated by the strength of the polyelectrolyte surface-potential for short-time colloidal deposition and by the decay range of the colloid-colloid repulsion for long-time colloidal deposition, i.e., while approaching to the saturation adsorption. In practice, the adsorption efficiency of the PDDA monolayer was tuned by increasing Δt_{PDDA} from 40 s to 2 min and, for given Δt_{PDDA}, Δt_{PS} was increased up to the achievement of saturated adsorption to drive the colloidal distribution across the conditions of the formulated electrostatic model.

On this basis, the following operative points are worth. First, the PDDA collector surface plays a role in the colloidal arrangement and its binding efficiency can be exploited as an effective mean for tuning the colloidal arrangement. Second, the interparticle spacing can be varied under not saturated adsorption conditions by means of the interplay between the adsorption times without loss of correlated disorder.

i) Since the adsorption times Δt_{PDDA} and Δt_{PS} play a key role in the implementation of the MNL-CL protocol, exploiting their interplay is a method easier than preparing multiple colloidal solutions differing for the screening length of Coulomb repulsion and/or concentration. In practice, the presence of salt is the less controllable parameter in terms of ordering and capillarity effects among the parameters allowing to tune d_{NN}.
ii) The flexible tuning of coverage over a wide interval (we have demonstrated coverage ranging from 9 to 33%) and ordering allowed by the MNL-CL protocol is particularly suitable to point out changes not only in the degree of correlated disorder but also in the local geometry coordination. Indeed, optimal conditions to retain correlated ordering over a wide range of values of d_{NN} enabled by the MNL-CL protocol also demonstrated to be a powerful tool to disclose changes in the geometry coordination of a short-range lattice and their impact on the spectral response of metal nanohole arrangements [58]. From the conceptual standpoint, FFT of the autocorrelation function has allowed us to discriminate the coverage threshold above which ordering is lost when salt is added to the colloid suspension. Such behavior has been demonstrated to be absent under salt-free conditions resulting from the optimization process underlying the MNL-CL protocol.
iii) We demonstrated that while the MNL-CL protocol enables to obtain correlated disorder for salt-free suspensions, the addition of salt causes a rapid evolution of the colloid distribution towards a total loss of order even under short-time colloid adsorption conditions. Using or ruling out salt-screening depends on the specific application. For instance, salt addition to the colloidal suspension may be undesirable in applications where d_{NN} is not required to decrease below a certain threshold, such as in the fabrication of nanohole arrays [56,57].

Hence, practical guidelines result from our experiments that can be useful in applications demanding a good level of correlated disorder and stringent constraints on d_{NN}.

Conclusions

In the framework of the colloidal lithography technique, supported monolayers of charged colloids are obtained by electrostatic binding to a counter-charged surface being usually a multilayer consisting of alternating oppositely charged polyelectrolytes.

In this study, we have discussed a modified colloidal lithography protocol, briefly termed MNL-CL protocol, developed to efficiently simplify and speed-up the conventional colloidal lithography deposition procedure based on a properly deposited single, rather than multi-layered, polyelectrolyte binding the colloidal mask. In detail, we have presented negatively charged PS nanospheres, with nominal diameter D_{PS}= 80 nm and 100 nm, electrostatically self-assembled onto a PDDA monolayer as a function of: i) adsorption time of PDDA (Δt_{PDDA}) from a salt-free aqueous solution with low enough concentration to favor extended chain conformation, ii) adsorption time of the PS nanospheres (Δt_{PS}) onto PDDA from an aqueous solution, and iii) ionic strength of the colloidal solution tuned by intentional addition of NaCl salt.

In order to investigate the conditions under which the presence of the PDDA and its deposition conditions can impact on the characteristics of the colloidal mask, we have developed and discussed a simple conceptual model that, depending on the surface charge associated with the colloidal diameter, predicts a threshold interparticle spacing (i.e., $L_{bb} = L_b + D_{PS}$ where $L_b = (e/2)\, D_{PS}$) below which the impact of the PDDA monolayer on the distribution of the colloids may be probed and, consequently, exploited in fabricating colloidal lithography masks.

Short-time deposition of colloids has enabled to probe the adsorption efficiency of the PDDA layer and long-time deposition of colloids has yielded stable rearrangement of the mask under the net electrostatic interaction, stemming from substrate and colloid charges. From the fundamental standpoint, our experimental findings have been found to be consistent with the predictions of the model.

Among the convenience and practical issues of the MNL-CL protocol, i) it is an actual and low cost simplification of the conventional colloidal lithography procedure using polyelectrolyte multilayers, ii) it provides distributions with well separated colloids and good degree of correlated disorder and iii) it points out the possibility to exploit the degree of saturation of the polyelectrolyte surface to drive and/or tuning the characteristics (coverage and ordering) of a short-range ordered colloidal mask

Definitively, the MNL-CL protocol paves the way to wide spread of colloidal lithography due to its: i) implementing colloidal lithography more easily than varying salt-related electrostatic screening and/or colloidal concentration, ii) exploiting the adsorption time of the collector surface as a further parameter for the optimization of colloidal lithography mask arrangements. and iii) using salt-free rather than electrolyte screened colloid suspensions combined with the advantages of the interplay between the adsorption times of the polyelectrolyte monolayer and colloids for controlling effectively the colloid distribution in terms of order, homogeneity and geometrical coordination over a wide range of fractional coverage.

As a further investigation, autocorrelation and Fast Fourier Transform (FFT) tools have been applied to introduce and measure a very short-range periodicity length-scale to be compared with the statistical interparticle spacing and able to characterize rigorously the occurrence of correlated disorder (i.e., short-range ordering) with respect to disordered arrangements. Moreover, as a practical demonstration of promising performances, advantages and potentialities of the MNL-CL protocol, we have fabricated nanohole distributions based on template colloidal masks made by the MNL-CL protocol and characterized their transmittance and refractive index sensing properties.

Declaration of Competing Interest

There are no conflicts to declare.

Acknowledgments

This work was supported by a grant from the Ministry of Education, University and Research (MIUR) for the scientific program SIR2014 Scientific Independence of young Researcher (RBSI1455LK).

The authors acknowledge Adriano Colombelli (IMM-CNR Lecce) for the sensing measurements, Enrico Melissano (IMM-CNR, Lecce) for the thermal deposition of gold films as well as Adriana Campa (IMM-CNR, Lecce) and Maria Concetta Martucci (IMM-CNR, Lecce) for oxygen plasma treatments, Antonio Pinna and Maurizio Russo for technical support for SEM analyses.

References

[1] W.L. Barnes, A. Dereux, T.W. Ebbesen, Surface plasmon subwavelength optics, Nature 424 (2003) 824–830, doi:10.1038/nature01937.
[2] C. Valsecchi, A.G. Brolo, Periodic metallic nanostructures as plasmonic chemical sensors, Langmuir 29 (2013) 5638–5649, doi:10.1021/la400085r.
[3] J.-.E. Park, Y. Jung, M. Kim, J.-.M. Nam, Quantitative nanoplasmonics, ACS Cent. Sci. 4 (2018) 1303–1314, doi:10.1021/acscentsci.8b00423.
[4] J.A. Schuller, E.S. Barnard, W. Cai, Y.C. Jun, J.S. White, M.L. Brongersma, Plasmonics for extreme light concentration and manipulation, Nat. Mater. 9 (2010) 193–204, doi:10.1038/nmat2630.
[5] M. Dragoman, D. Dragoman, Plasmonics: applications to nanoscale terahertz and optical devices, Prog. Quantum Electron. 32 (2008) 1–41, doi:10.1016/j.pquantelec.2007.11.001.
[6] V.G. Kravets, A.V. Kabashin, W.L. Barnes, A.N. Grigorenko, Plasmonic surface lattice resonances: a review of properties and applications, Chem. Rev. 118 (2018) 5912–5951, doi:10.1021/acs.chemrev.8b00243.
[7] S. Nie, S.R. Emory, Probing single molecules and single nanoparticles by surface-enhanced raman scattering, Science 275 (1997) 1102, doi:10.1126/science.275.5303.1102.
[8] A.G. Brolo, S.C. Kwok, M.G. Moffitt, R. Gordon, J. Riordon, K.L. Kavanagh, Enhanced fluorescence from arrays of nanoholes in a gold film, J. Am. Chem. Soc. 127 (2005) 14936–14941, doi:10.1021/ja0548687.
[9] M. Li, S.K. Cushing, N. Wu, Plasmon-enhanced optical sensors: a review, Analyst 140 (2015) 386–406, doi:10.1039/C4AN01079E.
[10] A.-.P. Blanchard-Dionne, M. Meunier, Sensing with periodic nanohole arrays, Adv. Optics Photon. 9 (2017) 891–940, doi:10.1364/AOP.9.000891.
[11] J.N. Anker, W.P. Hall, O. Lyandres, N.C. Shah, J. Zhao, R.P. Van Duyne, Biosensing with plasmonic nanosensors, Nat. Mater. 7 (2008) 442–453, doi:10.1038/nmat2162.
[12] X. Luo, T. Ishihara, Subwavelength photolithography based on surface-plasmon polariton resonance, Opt. Express 12 (2004) 3055–3065, doi:10.1364/OPEX.12.003055.
[13] Y. Gong, A.G. Joly, P.Z. El-Khoury, W.P. Hess, Interferometric plasmonic lensing with nanohole arrays, J. Phys. Chem. Lett. 5 (2014) 4243–4248, doi:10.1021/jz502296n.
[14] M. Kauranen, A.V. Zayats, Nonlinear plasmonics, Nat. Photonics 6 (2012) 737, doi:10.1038/nphoton.2012.244.
[15] E. Kretschmann, H.Notizen Raether, Radiative Decay of Non Radiative Surface Plasmons Excited by Light, Zeitschr. Naturforsch. A 23 (1968) 2135.
[16] W.L. Barnes, Surface plasmon–polariton length scales: a route to sub-wavelength optics, J. Opt. A Pure Appl. Opt. 8 (2006) S87–S93, doi:10.1088/1464-4258/8/4/s06.
[17] S.-.H. Chang, S.K. Gray, G.C. Schatz, Surface plasmon generation and light transmission by isolated nanoholes and arrays of nanoholes in thin metal films, Opt. Express 13 (2005) 3150–3165, doi:10.1364/OPEX.13.003150.
[18] D. Pacifici, H.J. Lezec, L.A. Sweatlock, R.J. Walters, H.A. Atwater, Universal optical transmission features in periodic and quasiperiodic hole arrays, Opt. Express 16 (2008) 9222–9238, doi:10.1364/OE.16.009222.
[19] I. Kaminska, T. Maurer, R. Nicolas, M. Renault, T. Lerond, R. Salas-Montiel, Z. Herro, M. Kazan, J. Niedziolka-Jönsson, J. Plain, et al., Near-field and far-field sensitivities of LSPR sensors, J. Phys. Chem. C 119 (2015) 9470–9476, doi:10.1021/acs.jpcc.5b00566.
[20] Y. Wang, L. Wu, T.I. Wong, M. Bauch, Q. Zhang, J. Zhang, X. Liu, X. Zhou, P. Bai, J. Dostalek, et al., Directional fluorescence emission co-enhanced by localized and propagating surface plasmons for biosensing, Nanoscale 8 (2016) 8008–8016, doi:10.1039/C5NR08816J.
[21] M. Couture, L.S. Live, A. Dhawan, J.-.F. Masson, EOT or Kretschmann configuration? Comparative study of the plasmonic modes in gold nanohole arrays, Analyst 137 (2012) 4162–4170, doi:10.1039/C2AN35566C.
[22] M.E. Stewart, C.R. Anderton, L.B. Thompson, J. Maria, S.K. Gray, J.A. Rogers, R.G. Nuzzo, Nanostructured plasmonic sensors, Chem. Rev. 108 (2008) 494–521, doi:10.1021/cr068126n.
[23] T. Ito, S. Okazaki, Pushing the limits of lithography, Nature 406 (2000) 1027–1031, doi:10.1038/35023233.
[24] J. Grand, P.-.M. Adam, A.-.S. Grimault, A. Vial, M.L. de la Chapelle, J.-.L. Bijeon, S. Kostcheev, P. Royer, Optical extinction spectroscopy of oblate, prolate and ellipsoid shaped gold nanoparticles: experiments and theory | SpringerLink, Plasmonics 1 (2006) 135–140, doi:10.1007/s11468-006-9014-7.
[25] T. Ohno, J.A. Bain, T.E. Schlesinger, Observation of geometrical resonance in optical throughput of very small aperture lasers associated with surface plasmons, J. Appl. Phys. 101 (2007) 083107, doi:10.1063/1.2718880.
[26] H.W. Deckman, J.H. Dunsmuir, Natural lithography, Appl. Phys. Lett. 41 (1982) 377–379, doi:10.1063/1.93501.
[27] U.C. Fischer, H.P. Zingsheim, Submicroscopic pattern replication with visible light, J. Vac. Sci. Technol. 19 (1981) 881–885, doi:10.1116/1.571227.
[28] P. Colson, C. Henrist, R. Cloots, Nanosphere lithography: a powerful method for the controlled manufacturing of nanomaterials, J. Nanomater. 2013 (2013).
[29] J.-.F. Masson, M.-.P. Murray-Méthot, L.S. Live, Nanohole arrays in chemical analysis: manufacturing methods and applications, Analyst 135 (2010) 1483–1489, doi:10.1039/C0AN00053A.
[30] Y. Min, M. Akbulut, K. Kristiansen, Y. Golan, J. Israelachvili, The role of interparticle and external forces in nanoparticle assembly, Nat. Mater. 7 (2008) 527–538, doi:10.1038/nmat2206.
[31] P. Hanarp, D.S. Sutherland, J. Gold, B. Kasemo, Control of nanoparticle film structure for colloidal lithography, Colloids Surf. A 214 (2003) 23–36, doi:10.1016/S0927-7757(02)00367-9.
[32] P. Hanarp, D. Sutherland, J. Gold, B. Kasemo, Nanostructured model biomaterial surfaces prepared by colloidal lithography, Nanostruct. Mater. 12 (1999) 429–432, doi:10.1016/S0965-9773(99)00151-8.
[33] Z. Adamczyk, P. Warszyński, Role of electrostatic interactions in particle adsorption, Adv. Colloid Interface Sci. 63 (1996) 41–149, doi:10.1016/0001-8686(95)00281-2.
[34] C.L. Haynes, R.P. Van Duyne, Nanosphere lithography: a versatile nanofabrication tool for studies of size-dependent nanoparticle optics, J. Phys. Chem. B 105 (2001) 5599–5611, doi:10.1021/jp010657m.
[35] M. Duval Malinsky, K.L. Kelly, G.C. Schatz, R.P. Van Duyne, Nanosphere lithography: effect of substrate on the localized surface plasmon resonance spectrum of silver nanoparticles, J. Phys. Chem. B 105 (2001) 2343–2350, doi:10.1021/jp002906x.
[36] B.J.Y. Tan, C.H. Sow, T.S. Koh, K.C. Chin, A.T.S. Wee, C.K Ong, Fabrication of size-tunable gold nanoparticles array with nanosphere lithography, reactive ion etching, and thermal annealing, J. Phys. Chem. B 109 (2005) 11100–11109, doi:10.1021/jp045172n.
[37] M.-.P. Murray-Methot, N. Menegazzo, J.-.F. Masson, Analytical and physical optimization of nanohole-array sensors prepared by modified nanosphere lithography, Analyst 133 (2008) 1714–1721, doi:10.1039/B808820A.
[38] D.-.G. Choi, H.K. Yu, S.G. Jang, S.-.M. Yang, Colloidal lithographic nanopatterning via reactive ion etching, J. Am. Chem. Soc. 126 (2004) 7019–7025, doi:10.1021/ja0319083.
[39] D.-.G. Choi, S. Kim, E. Lee, S.-.M. Yang, Particle arrays with patterned pores by nanomachining with colloidal masks, J. Am. Chem. Soc. 127 (2005) 1636–1637, doi:10.1021/ja044578a.

[40] C.L. Haynes, A.D. McFarland, M.T. Smith, J.C. Hulteen, R.P. Van Duyne, Angle-resolved nanosphere lithography: manipulation of nanoparticle size, shape, and interparticle spacing, J. Phys. Chem. B 106 (2002) 1898–1902 10.1021/jp013570+.
[41] I. Szilagyi, G. Trefalt, A. Tiraferri, P. Maroni, M. Borkovec, Polyelectrolyte adsorption, interparticle forces, and colloidal aggregation, Soft Matter 10 (2014) 2479–2502, doi:10.1039/C3SM52132J.
[42] G. Decher, J.-.D. Hong, Buildup of ultrathin multilayer films by a self-assembly process, 1 consecutive adsorption of anionic and cationic bipolar amphiphiles on charged surfaces, Makromol. Chem. Macromol. Symp. 46 (1991) 321–327, doi:10.1002/masy.19910460145.
[43] T. Serizawa, H. Takeshita, M. Akashi, Electrostatic adsorption of polystyrene nanospheres onto the surface of an ultrathin polymer film prepared by using an alternate adsorption technique, Langmuir 14 (1998) 4088–4094, doi:10.1021/la9713661.
[44] C. Acikgoz, M.A. Hempenius, J. Huskens, G.J. Vancso, Polymers in conventional and alternative lithography for the fabrication of nanostructures, Eur. Polym. J. 47 (2011) 2033–2052, doi:10.1016/j.eurpolymj.2011.07.025.
[45] A. Ge, M. Matsusaki, L. Qiao, M. Akashi, S. Ye, Salt effects on surface structures of polyelectrolyte multilayers (PEMs) investigated by vibrational sum frequency generation (SFG) spectroscopy, Langmuir 32 (2016) 3803–3810, doi:10.1021/acs.langmuir.5b04765.
[46] S. Lee, D. Kim, S.-.M. Kim, J.-.A. Kim, T. Kim, D.-.Y. Kim, M.-.H. Yoon, Polyelectrolyte multilayer-assisted fabrication of non-periodic silicon nanocolumn substrates for cellular interface applications, Nanoscale 7 (2015) 14627–14635, doi:10.1039/C5NR02384J.
[47] M. Schönhoff, Layered polyelectrolyte complexes: physics of formation and molecular properties, J. Phys. Condens. Matter 15 (2003) R1781–R1808, doi:10.1088/0953-8984/15/49/r01.
[48] B. Wu, C. Li, H. Yang, G. Liu, G. Zhang, Formation of polyelectrolyte multilayers by flexible and semi-flexible chains, J. Phys. Chem. B 116 (2012) 3106–3114, doi:10.1021/jp212621h.
[49] R.A. McAloney, M.C. Goh, In situ investigations of polyelectrolyte film formation by second harmonic generation, J. Phys. Chem. B 103 (1999) 10729–10732, doi:10.1021/jp9925740.
[50] O. Mermut, C.J. Barrett, Effects of charge density and counterions on the assembly of polyelectrolyte multilayers, J. Phys. Chem. B 107 (2003) 2525–2530, doi:10.1021/jp027278t.
[51] J.J. Gray, R.T. Bonnecaze, Adsorption of colloidal particles by Brownian dynamics simulation: kinetics and surface structures, J. Chem. Phys. 114 (2001) 1366–1381, doi:10.1063/1.1319317.
[52] H. Fredriksson, Y. Alaverdyan, A. Dmitriev, C. Langhammer, D.S. Sutherland, M. Zäch, B. Kasemo, Hole–mask colloidal lithography, Adv. Mater. 19 (2007) 4297–4302, doi:10.1002/adma.200700680.
[53] S. Syrenova, C. Wadell, C. Langhammer, Shrinking-hole colloidal lithography: self-aligned nanofabrication of complex plasmonic nanoantennas, Nano Lett. 14 (2014) 2655–2663, doi:10.1021/nl500514y.
[54] C. Wadell, C. Langhammer, Drift-corrected nanoplasmonic hydrogen sensing by polarization, Nanoscale 7 (2015) 10963–10969, doi:10.1039/C5NR01818H.
[55] Y. M. Lvov, J. F. Rusling, D. Laurence Thomsen, F. Papadimitrakopoulos, T. Kawakami, T Kunitake, High-speed multilayer film assembly by alternate adsorption of silica nanoparticles and linear polycation, Chem. Commun. (1998) 1229–1230, doi:10.1039/A801456F.
[56] M. Cesaria, A. Taurino, M.G. Manera, M. Minunni, S. Scarano, R. Rella, Gold nanoholes fabricated by colloidal lithography: novel insights into nanofabrication, short-range correlation and optical properties, Nanoscale 11 (2019) 8416–8432, doi:10.1039/C8NR09911A.
[57] M. Cesaria, A. Colombelli, D. Lospinoso, A. Taurino, E. Melissano, R. Rella, G.M. Manera, Long - and short-range ordered gold nanoholes as large-area optical transducers in sensing applications, Chemosensors 7 (2019), doi:10.3390/chemosensors7010013.
[58] M. Cesaria, A. Taurino, M.G. Manera, R. Rella, Short-range ordered 2D nanoholes: lattice-model and novel insight into the impact of coordination geometry and packing on their propagating-mode transmittance features, Nanoscale Advances 2 (2020) 4133–4146, doi:10.1039/D0NA00449A.
[59] N.M. Doskaliuk, Khalavka Y.B F.P.M., Effect of conditions for formation of nanocomposite films of poly (diallyldimethylammonium chloride) – CdTe/CdS nanocrystals on their structure and optical density | SpringerLink, Theor. Exp. Chem. (2016) 52, doi:10.1007/s11237-016-9454-x.
[60] C. Gao, S. Leporatti, E. Donath, H. Möhwald, Surface texture of poly(styrenesulfonate sodium salt) and poly(diallyldimethylammonium chloride) micron-sized multilayer capsules: a scanning force and confocal microscopy study, J. Phys. Chem. B 104 (2000) 7144–7149, doi:10.1021/jp000615i.
[61] Z. Adamczyk, K. Jamroży, P. Batys, A. Michna, Influence of ionic strength on poly(diallyldimethylammonium chloride) macromolecule conformations in electrolyte solutions, J. Colloid Interface Sci. 435 (2014) 182–190, doi:10.1016/j.jcis.2014.07.037.
[62] R.A. McAloney, M. Sinyor, V. Dudnik, M.C. Goh, Atomic force microscopy studies of salt effects on polyelectrolyte multilayer film morphology, Langmuir 17 (2001) 6655–6663, doi:10.1021/la010136q.
[63] A. Thill, O. Spalla, Aggregation due to capillary forces during drying of particle submonolayers, Colloids Surf. A 217 (2003) 143–151, doi:10.1016/S0927-7757(02)00569-1.
[64] J. Aizenberg, P.V. Braun, P. Wiltzius, Patterned colloidal deposition controlled by electrostatic and capillary forces, Phys. Rev. Lett. 84 (2000) 2997–3000, doi:10.1103/PhysRevLett.84.2997.
[65] M. Miyahara, S. Watanabe, Y. Gotoh, K. Higashitani, Adsorption and order formation of colloidal nanoparticles on a substrate: a Brownian dynamics study, J. Chem. Phys. 120 (2004) 1524–1534, doi:10.1063/1.1632896.
[66] B. Derjaguin, L. Landau, Theory of the stability of strongly charged lyophobic sols and of the adhesion of strongly charged particles in solutions of electrolytes, Prog. Surf. Sci. 43 (1993) 30–59, doi:10.1016/0079-6816(93)90013-L.
[67] E.J.W Verwey, Theory of the stability of lyophobic colloids, J. Phys. Colloid Chem. 51 (1947) 631–636, doi:10.1021/j150453a001.
[68] D. Grasso*, K. Subramaniam, M. Butkus, K. Strevett, J Bergendahl, A review of non-DLVO interactions in environmental colloidal systems, Rev. Environ. Sci. Biotechnol. 1 (2002) 17–38, doi:10.1023/A:1015146710500.
[69] E.M.V. Hoek, G.K Agarwal, Extended DLVO interactions between spherical particles and rough surfaces, J. Colloid Interface Sci. 298 (2006) 50–58, doi:10.1016/j.jcis.2005.12.031.
[70] L. Du, S. Zhang, G. Chen, G. Yin, C. Du, Q. Tan, Y. Sun, Y. Qu, Y. Gao, Polyelectrolyte assisted synthesis and enhanced oxygen reduction activity of Pt nanocrystals with controllable shape and size, ACS Appl. Mater. Interfaces 6 (2014) 14043–14049, doi:10.1021/am503372f.
[71] F. Przybilla, C. Genet, T.W. Ebbesen, Long vs. short-range orders in random subwavelength hole arrays, Opt. Express 20 (2012) 4697–4709, doi:10.1364/OE.20.004697.
[72] S., .B.. Malani, P Viswanath, Impact of ordering of gold nanohole arrays on refractive index sensing, J. Optic. Soc. Am. B 35 (2018) 2501–2508, doi:10.1364/JOSAB.35.002501.